Were early Archean carbonate factories major carbon sinks on the juvenile Earth?

Xiang, Wanli[1, 2], Duda, Jan-Peter[2], Pack, Andreas[3], van Zuilen, Mark[4], Reitner, Joachim[2, 5]

[1] College of Tourism and Geographical Science, Leshan Normal University, Leshan, 614000, China.

[2] Department of Geobiology, University of Göttingen, Göttingen, 37077, Germany.

[3] Department of Geochemistry and Isotope Geology, University of Göttingen, Göttingen, 37077, Germany.

[4] CNRS-UMR6538 Laboratoire Geo-Ocean, Institut Universitaire Européen de la Mer (IUEM), Université de Bretagne Occidentale, Plouzané, 29280, France.

[5] Göttingen Academy of Science and Humanities in Lower Saxony, Göttingen, 37073, Germany.

Correspondence to: Reitner Joachim (jreitne@gwdg.de)

Abstract. Paleoarchean carbonates in the Pilbara Craton (Western Australia) are important archives for early life and environment on early Earth. Amongst others, carbonates occur in interstitial spaces of ca. 3.5–3.4 Ga pillow basalts (North Star-, Mount Ada-, Apex-, and Euro Basalt, Dresser Formation) and associated with bedded deposits (Dresser- and Strelley Pool Formation, Euro Basalt). This study aims to understand the formation and geobiological significance of those early Archean carbonates by investigating their temporal-spatial distribution, petrography, mineralogy, and geochemistry (e.g., trace elemental compositions, $\delta^{13}C$, $\delta^{18}O$). Three carbonate factories are recognized: (i) an oceanic crust factory, (ii) an organo-carbonate factory, and (iii) a microbial carbonate factory. The oceanic crust factory is characterized by carbonates formed in interspaces between pillowed basalts ("interstitial carbonates"). These carbonates precipitated inorganically on and within the basaltic oceanic crust from CO_2-enriched seawater and seawater-derived alkaline hydrothermal fluids. The organo-carbonate factory is characterized by carbonate precipitates that are spatially associated with organic matter. The close association with organic matter suggests that the carbonates formed taphonomically via organo-mineralization, that is, linked to organic macromolecules (either biotic or abiotic) which provided nucleation sites for carbonate crystal growth. Organo-carbonate associations occur in a wide variety of hydrothermally influenced settings, ranging from shallow marine environments to terrestrial hydrothermal ponds. The microbial carbonate factory includes carbonate precipitates formed through mineralization of extracellular polymeric substances (EPS) associated with microbial mats and biofilms. It is commonly linked to shallow subaquatic environments, where (anoxygenic) photoautotrophs might have been involved in carbonate formation. In case of all three carbonates factories, hydrothermal fluids seem to play a key-role in the formation and preservation of mineral precipitates. For instance, alkaline earth metals and organic materials delivered by fluids may promote carbonate precipitation, whilst soluble silica in the fluids drives early chert formation, delicately preserving

authigenic carbonate precipitates and associated features. Regardless of the formation pathway, Paleoarchean carbonates might have been major carbon sinks on the early Earth, modulating the carbon cycle and, hence, climate variability.

1 Introduction

35   Carbonate factories are conceptual models encompassing carbonate production and associated processes at various scales, from local precipitation to global sedimentation (Schlager, 2000; Schrag et al., 2013; Reijmer, 2021). Throughout most of Earth's history, carbonate precipitation has been closely linked to biological processes, ranging from direct to indirect precipitation (that is, biologically controlled vs induced) (Flügel, 2010). Over the past couple of years, awareness has risen that carbonate precipitation can also be induced by organic matter (i.e., "organo-mineralization"), regardless of its origin

40   (Addadi and Weiner, 1985; Reitner, 1993; Reitner et al., 1995a, b, 2000, 2001; Trichet and Défarge, 1995; Pei et al., 2021). Based on previous works about "cold-water carbonates" (Lees and Buller, 1972) and "mud-mound carbonates" (Reitner and Neuweiler, 1995), Schlager (2000) summarized three modern carbonate factories in the marine benthic zone, namely tropical shallow-water system, cool and deep-water system, and mud-mound/microbial buildup system. Since then, the carbonate factory concept has been extended across spatial and temporal scales (Pomar and Hallock, 2008; Reijmer, 2021; Pei et al,

45   2021; Wang et al., 2023).

Although skeletal, CaCO$_3$-forming eukaryotes only evolved in the latest Ediacaran (e.g. *Cloudina*: Germs, 1972; Grant, 1990), carbonate deposits are widespread throughout the Precambrian (e.g., Grotzinger and Knoll, 1995; Grotzinger and James, 2000; Veizer, 1989a, b; Cantine et al., 2020). Particularly notable is the potential *in situ* precipitation of authigenic carbonates on the seafloor, which is only very rarely known from the Phanerozoic, where it seems to be driven by elevated

50   CaCO$_3$ saturation of seawater associated with widespread anoxia (Grotzinger and Knoll, 1995; Copper, 2002; Pruss et al., 2006; Knoll et al., 2007; Higgins et al. 2009; Pei et al., 2019, 2023; Lu et al., 2023). Proposed mechanisms for carbonate formation, prior to the advent of biomineralization in the terminal Precambrian, include a variety of poorly constrained abiotic and microbial processes (Grotzinger and James, 2000). As a result, the underlying carbonate factories are still poorly understood, which is particularly true for the early Archean, when life still was in its infancy.

55   The earliest putative traces of life on our planet are preserved in a variety of different rock types, including banded iron formation (BIF), cherts, as well as (silicified) siliciclastic and carbonate sedimentary rocks (e.g. Van Kranendonk, 2006, 2007; Lepot, 2020). Many of those putative records can be found in the ca. 4.0–3.6 Ga Isua Supracrustal Belt (ISB; West Greenland), the 3.5–3.2 Ga East Pilbara Terrane (EPT; Pilbara Craton, Western Australia), and the 3.6–3.2 Ga Barberton Greenstone Belt (BGB; South Africa). In contrast to the highly metamorphic - amphibolitic ISB, rocks of the EPT and BGB

60   only underwent regional metamorphism from prehnite-pumpellyite (100–250 °C) to lower greenschist facies (250–300 °C) (Nutman et al., 2019a, b; Van Kranendonk et al., 2019a; Hickman-Lewis et al., 2019).

Rocks of the EPT and BGB show evidence of pervasive carbonatization and silicification by seawater and/or hydrothermal fluids (Kitajima et al., 2001; Nakamura and Kato, 2002, 2004; Terabayashi et al., 2003; Hofmann and Harris, 2008;

Hickman-Lewis et al., 2019). At the same time, however, they also preserve primary carbonate precipitates, which may

65   provide important clues to early life and the physicochemical conditions in its habitats. Indeed, for decades researchers have

focused on carbonates associated with microbial facies in the ~3.4 Ga Strelley Pool Formation, preserving a wealth of

geobiologically significant textural and (bio)geochemical information (e.g., trace elemental compositions, $\delta^{13}C$, $\delta^{18}O$) (Van

Kranendonk, 2006, 2007; Allwood et al., 2006a, 2007, 2009; Marshall et al., 2007; Wacey, 2010; Bontognali et al, 2012;

Duda et al., 2016; Flannery et al., 2018; Sengupta et al., 2020). Notably, however, these carbonates are a minor component

70   in the EPT lithostratigraphy (Van Kranendonk et al., 2007b). The geobiological significance of other carbonates, such as

precipitates in the interspaces of (ultra)mafic rocks that possibly formed through seafloor hydrothermal alteration (referred to

as "interstitial carbonates" in this work) (Kitajima et al., 2001; Nakamura and Kato, 2002, 2004; Terabayashi et al., 2003;

Marien et al., 2023), remains poorly constrained.

This study comprehensively investigates early Archean carbonates in the EPT, including interstitial carbonates associated

75   with basalts, carbonate stromatolites and other sedimentary carbonates. The combination of detailed petrography with

mineralogical and geochemical analyses (e.g., trace elemental compositions, $\delta^{13}C$, $\delta^{18}O$) provides novel insights into the

formation of carbonates during the early Archean. The results of this study demonstrate the presence of various types of

carbonate factories on the juvenile Earth which might have been major carbon sinks and thus played a significant role in the

early global carbon cycle and, hence, climate system.

80   **2 Geological settings**

The EPT (3.53–3.17 Ga) in Western Australia is famous for its well-preserved Paleoarchean volcano-sedimentary

successions, which provide the world's most complete record of the evolution of the geo-, hydro-, bio- and atmosphere on

the early Earth (Van Kranendonk et al., 2007a, b; Hickman and Van Kranendonk, 2012a, b). A particular interest is the

Pilbara Supergroup, a 20 km thick succession of mainly volcanic rocks that can be subdivided into (from bottom to top) the

85   Warrawoona Group (3.53–3.43 Ga), the Kelly Group (3.42–3.32 Ga), the Sulphur Springs Group (3.27–3.23 Ga), and the

Soanesville Group (ca. 3.19 Ga) (Van Kranendonk et al., 2002, 2007b; Rasmussen et al., 2007; Hickman and Van

Kranendonk, 2012a, b). The lower three groups comprise ultramafic to felsic volcanic rocks, chemical and clastic deposits,

as well as swarms of subseafloor hydrothermal silica ± barite veins (Van Kranendonk, 2006). The tectonic setting of the EPT

is controversial, ranging from mid-ocean ridge and island arc (Ueno et al., 2001; Komiya et al., 2002; Kato and Nakamura,

90   2003) to a thick ocean volcanic plateau (Smithies et al., 2003, 2005, 2007a, b; Van Kranendonk, 2006; Van Kranendonk et

al., 2007a, b, 2019a).

A characteristic feature of the EPT is the so-called dome-and-keel structure, consisting of a central nucleus consisting of the

3459 ± 18 Ma North Pole Monzogranite ("North Pole Dome") surrounded by little-deformed, predominantly mafic volcanic

rocks of the Warrawoona Group and Kelly Group (Hickman and Van Kranendonk, 2012a) (Fig. 1). The oldest basaltic

95   formation in this area is the North Star Basalt (3490 ±15 Ma Ar/Ar), which is overlain by the Dresser Formation (3481 ± 2

Ma U-Pb) consisting of chert ± barite beds and veins that are associated with pillowed basalts and dolerite (Van Kranendonk et al., 2008; Hickman and Van Kranendonk, 2012b). Atop the Dresser Formation follows (from base to top) a ~ 4 km thick succession of mafic volcanic rocks (Mount Ada Basalt), a < 1.3 km thick succession of felsic volcanic rocks (Duffer Formation, Panorama Formation), and a < 150 m thick package of jasper (Marble Bar Chert Member, Towers Formation)

100 (Byerly et al., 2002; Hickman and Van Kranendonk, 2012b). In the eastern part of the dome, the Panorama Formation is underlain by the Apex basalt (Nakamura and Kato, 2004), which is dated to 3463–3454 Ma based on zircon U-Pb ages of the underlying Duffer Formation and the overlying Panorama Formation (Thorpe et al., 1992; McNaughton et al., 1993). Surrounding the central dome, the Panorama Formation is disconformably overlain by the Strelley Pool Formation (SPF, 3414 ± 34 Ma, U–Pb ages, Gardiner et al., 2019), which is known for its distinctive stromatolites (e.g., Lowe, 1980, 1983;

105 Hofmann et al., 1999; Van Kranendonk et al., 2003; Allwood et al., 2006a; Hickman et al., 2011; Duda et al., 2016), followed by the high-Mg and tholeiitic Euro Basalt (3350 ± 3 – 3335 ± 7 Ma, GSWA, 2013) (Van Kranendonk et al., 2006; Hickman and Van Kranendonk, 2012b).
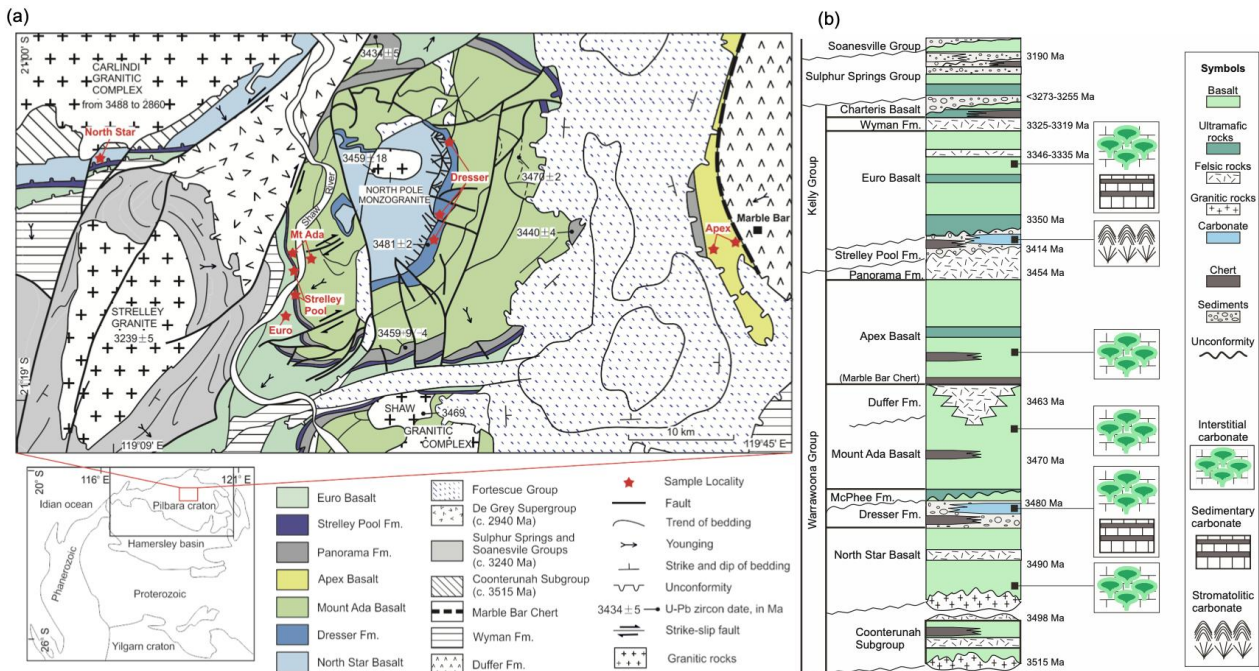
Figure 1: (a) Simplified geological map of the North Pole Dome, Eastern Pilbara Terrane, Western Australia (adapted from Van
110 **Kranendonk and Hickman, 2000, Hickman and Van Kranendonk, 2012b) including sampling localities (red stars). (b) Simplified**
stratigraphy of the studied Archean rocks (adapted from Van Kranendonk et al., 2007b).

3 Materials and methods

3.1 Sample locality

Paleoarchean carbonate rocks analyzed in this study derive from the North Pole Dome in the EPT (Fig. 1) and were collected
from existing drill cores stored at the Geological Survey of Western Australia (Agouron Institute Drilling Project, AIDP) as
well as during field campaigns organized by the German Research Foundation (DFG) Priority Program 1883 "Building a
Habitable Earth" together with Australian colleagues. Interstitial carbonates were sampled from the ~3.49 Ga North Star
Basalt (drill core 102 AIDP-1; 21°06'38"S, 119°06'4"E, French et al., 2015), the ~3.46 Ga Apex Basalt ("Schopf Locality"
at Chinaman Creek; Schopf, 1993), the ~3.47 Ga Mount Ada Basalt and the ~3.35 Ga Euro Basalt (both near "Trendall
Locality" at Shaw River; Hickmann et al., 2011), as well as from the Middle Basalt Member of ~3.48 Ga Dresser Formation
(Dresser Barite Mine). Bedded sedimentary carbonates were sampled from the Dresser Formation at the "Tsunami Locality"
(Runge et al. 2022) near the Dresser Barite Mine, and the Euro Basalt at the east side of the Shaw River near the "Trendall
Locality". Stromatolitic carbonates were collected from the Strelley Pool Formation at the western side of Shaw River.
For comparison, we additionally analyzed carbonate inclusions in black barites from the Dresser Formation (drill cores PDP
2b and 2c), rhodochrosites in cherts from the ~3.25 Ga Fig Tree Group (Heinrichs, 1980; Rincon-Thomas et al 2016),
carbonates of debated origin in the vicinity of the controversial ~3.7 Ga stromatolite site in the ISB in Greenland (Nutman et
al., 2016; Allwood et al., 2018; provided by van Zuilen, 2018), as well as carbonatites from ~540 Ma Fen Complex in
Norway (Andersen and Taylor, 1988) and the ~16 Ma Kaiserstuhl Volcanic Complex in Germany (Kraml et al., 2006).

3.2 Methods

3.2.1 Petrography and geochemical imaging

Petrographic thin sections were prepared (polished to approximately 60 μm thickness) for all samples and examined using a
Zeiss SteREO Discovery V12 stereomicroscope coupled with an AxioCam MRc camera. Selected carbonates were
additionally analyzed with a Cathodoluminescence (CL) microscope. CL images were acquired with a Cambridge
Instruments Citl CCL 8200 Mk3A cold-cathode system linked to a Zeiss Axiolab microscope (operating voltage of
approximately 15 kV and electric current of approximately 250-300 μA) and a Zeiss AxioCam 703 camera.
Minerals were identified by their optical characteristics and Raman spectroscopy, using a Horiba Jobin-Yvon LabRam-HR
800 UV spectrometer with a focal length of 800 mm and an excitation wavelength of 488 nm produced by an Argon ion laser
(Melles Griot IMA 106020B0S) and with a WITec alpha300 R fibre-coupled ultra-high throughput spectrometer. The former
spectrometer was calibrated using a silicon standard with a major peak at 520.4 cm^{-1}, and the spectra were processed using
software Fityk (Wojdyr, 2010) and comparatively analyzed based on references from the RRUFF database.
Element distributions were mapped using a Bruker M4 Tornado micro-X-ray fluorescence (micro-XRF) instrument equipped
with a XFlash 430 Silicon Drift Detector. Measurements were performed at a voltage of 50 kV and a current of 400 μA with
a spot size of 20 μm and a chamber pressure of 20 mbar.

3.2.2 Stable carbon and oxygen isotopes (δ^{13}C, δ^{18}O)

145 For stable isotope analyses, sample chips (diameter ~1 cm) were obtained from pristine areas (i.e., free of visible alteration, inclusions, and secondary porosity) using a microdrill. The sample chips were cleaned with ethanol using ultrasound (3x) and gently dried at room temperature before being crushed into small pieces. Carbonate was then picked out and powdered in an agate mortar and well homogenized. Additionally, some carbonate facies, including carbonate veinlets and carbonate inclusions, were extracted using a high-precision drill from individual mineral phases from polished rock slabs.

150 Carbon and oxygen stable isotopes of the carbonates were measured at 70 °C using a Thermo Scientific Kiel IV carbonate device coupled with a Finnigan DeltaPlus gas isotope mass spectrometer at the Geoscience Center of the Georg-August-Universität Göttingen. All results were normalized as delta values $\delta^{13}C_{carb}$ and $\delta^{18}O_{carb}$ relative to the Vienna PeeDee Belemnite (VPDB) reference standard. The standard deviation is better than 0.03 ‰ for $\delta^{13}C_{carb}$ and 0.05 ‰ for $\delta^{18}O_{carb}$, calculated by multiple measurements of the in-house carbonate standard Solnhofen.

155 4 Results

4.1 Interstitial carbonates

4.1.1 Host basalts

The host basalts are pillow-shaped, internally subdivided in more crystalline interiors and quenched glassy rims, and commonly locally cut by tectonic fractures (Fig. 2). The interspaces and fractures are filled with carbonate minerals and 160 chert. In most outcrops, the host basalts and interstitial carbonate minerals are weathered, resulting in orange to brownish colors.

Figure 2: Outcrop photos of Archean pillow basalts from the North Pole Dome, Eastern Pilbara Terrane, Western Australia. The pillows consist of relatively unaltered cores surrounded by quenched rims (black arrows), indicating a sub-aquatic formation.
165 **Interspaces between pillows are filled with carbonate minerals ("interstitial carbonate"; white arrows). (a) Outcrop of surficially weathered 3.49 Ga North Star Basalt with interspaces filled by Fe-dolomite and chert cement; (b) Outcrop of surficially weathered 3.48 Ga Dresser Formation lacking interstitial calcite due to weathering; (c) Outcrop of surficially weathered 3.47 Ga Mount Ada Basalt with interspaces filled by fibrous isopachous Fe-dolomite (brown colours, due to weathering) and white chert. It is locally cut by deep carbonate veins shown in (d), implying later fluid circulation. (e) Outcrop of little weathered 3.46 Ga Apex Basalt with**
170 **interspaces filled with pink calcite, basaltic breccia and minor chert. (f) Outcrop of little weathered ~3.35 Ga Euro Basalt with interspaces and fractures filled by pink calcite. The lengths of the brown and blue hammers are ca. 30 cm and ca. 40 cm, respectively. Scale bars are 10 cm in (c) and 20 cm in (d), respectively.**

Although the host basalts show secondary mineral assemblages indicative of greenschist metamorphism (calcite + chlorite + anatase + quartz ± pyrite), phenocrysts (i.e., plagioclase and pyroxene) can still be recognized in the basalt interior of the
175 well-preserved samples, e.g. A22 from the Apex Basalt (Figs. 3a, 4a). Notably, the well-preserved basalts exhibit concentric green ophitic-holohyaline interiors and yellow-green quenched margins. In the margins, the size and density of ovoid spherulites and variolites (amygdules) decrease outwards, merging into the glassy zone (Fig. S1a-c). Spherulitic and variolitic zones in the basalts are highly carbonatized, with carbonate minerals being particularly prominent in variolites and concentric syngenetic veins. Notably, elemental distributions in basalts do not seem to relate to the degree of weathering (e.g.
180 in sample A22 of the Apex Basalt; Fig. 3b) and hence might be pristine. Except for the devitrified volcanic glass, Si is rich in the interior of the pillow basalt but rare in the zone of spherulites and variolites, which are dominated by calcite.

In case of altered host basalts, progressive deformation and metamorphism are evidenced by the migration and breakup of secondary minerals (e.g. chlorite), erased volcanic textures, as well as by the presence of schistose areas (Figs. 5a, S1d-i). The migration of chlorite, which is a dominant Fe-bearing secondary mineral, caused a loss of Fe in weathered basalts (Fig.
185 5a). Minerals of the chlorite-group frequently occur in interstitial carbonates close to, and within, tectonic fractures in the pillow basalts (Fig. 5b).
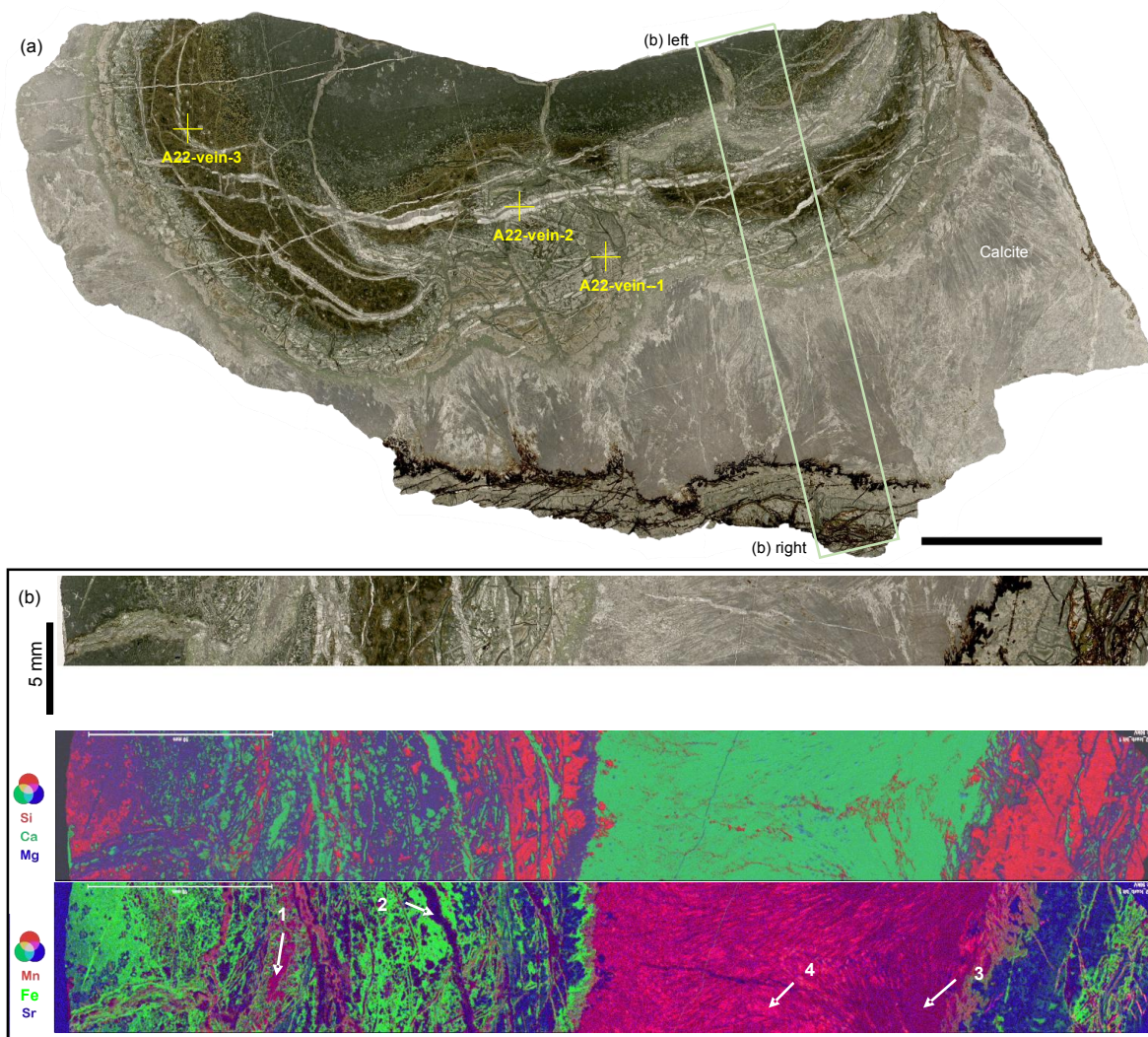
Figure 3: (a) Thin section scan image (transmitted light) of sample A22 from the Apex Basalt, showing concentric pillow structures of the basalt and well-preserved primary acicular crystal-fans of interstitial carbonates (mainly calcite). Yellow crosses mark the positions of subsamples analysed for stable oxygen and carbon isotopes (Table 1, Fig. S3). The scale bar in (a) is 20 mm. (b) Blow-up image and µXRF mappings of rectangle area highlighted in (a). The false-colour overlapping image of Si (red), Ca (green) and Mg (blue) in the middle panel is well in line with interspaces dominantly filled by calcite with minor chert. In addition, the quenched margin of the basalt seems to relatively depleted in Si as compared to the core, implying a loss of Si during carbonatization processes. The Si yielded by carbonatization was likely enriched in fluids and resulted in the later cementation of interstitial calcite by chert. The false-colour overlapping image of Mn (red), Fe (green) and Sr (blue) in the lower panel highlights the presence of four calcite facies, that is, Mn-enriched syngenetic veins (white arrow 1), Mn-depleted later veins (white arrow 2), Mn-depleted acicular interstitial calcite (white arrow 3), and Mn-enriched calcite cement (white arrow 4). The images of each element are shown in Fig. S5.
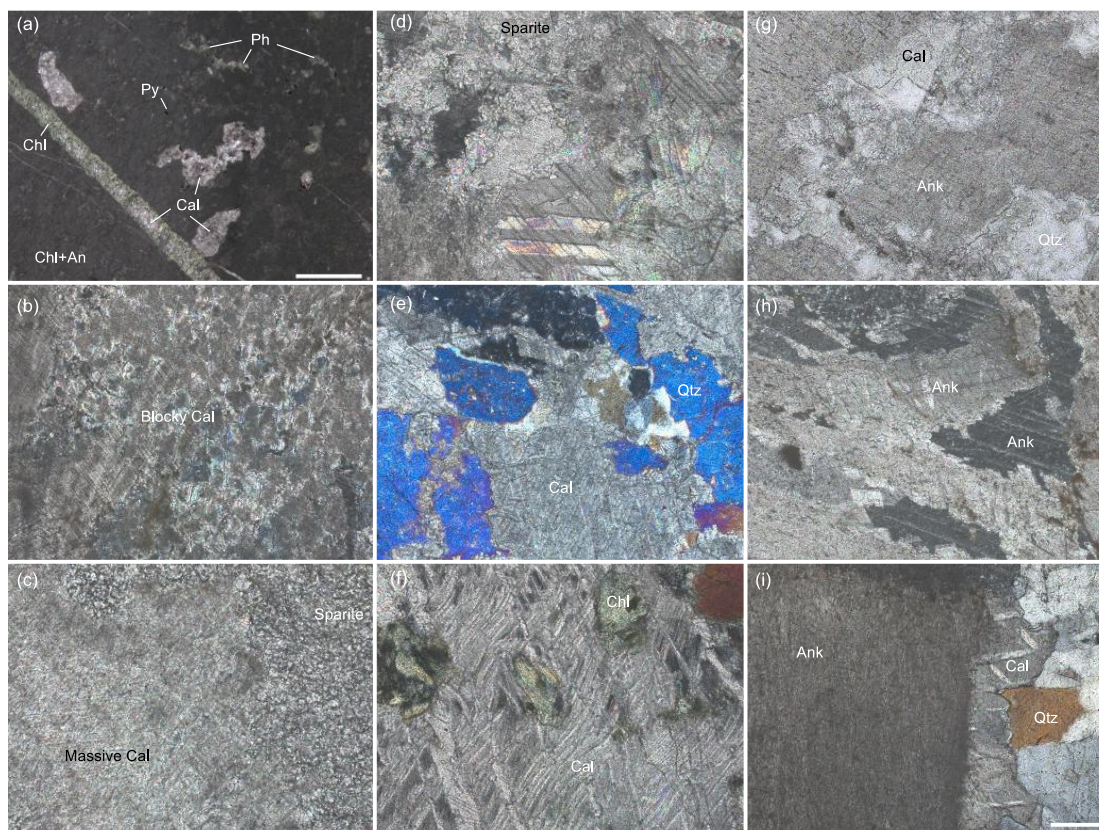
200 **Figure 4: Thin section photographs of altered interstitial carbonates from the North Pole Dome, Eastern Pilbara Terrane, Western Australia. (a) Phenocrysts can be recognized in the well-preserved host basalt, although the secondary mineral assemblage is indicative of greenschist metamorphism (calcite + chlorite + anatase + quartz ± pyrite). The acicular crystal-fan calcite is altered to blocky calcite (b) as well as to massive and sparitic calcite (c). (d) Large sparitic crystals in a wide fracture. (e) The blocky calcites are cemented by quartz. (f) Metamorphic S-C fabrics of sparite and chlorite crystals indicate dynamic metamorphism. (g) Blocky**
205 **ankerites often show calcite overgrowths at their edges. (h) Some ankerites exhibit features formed by recrystallization and neomorphism. (i) Along dewatering cracks, ankerites in deep carbonate veins are commonly overgrown by calcite and chert cement. (a) to (c): Apex Basalt; (d): Dresser Formation; (e) and (f): Euro Basalt; (g) to (i): Mount Ada Basalt. All photos except (g) were taken under cross-polarized light. Scale bar in (i) corresponds to 200 μm and is applicable to all photographs. Abbreviations: Ph-phenocryst, Cal-calcite, Chl- chlorite, Qtz- quartz, Ank-ankerite.**

210
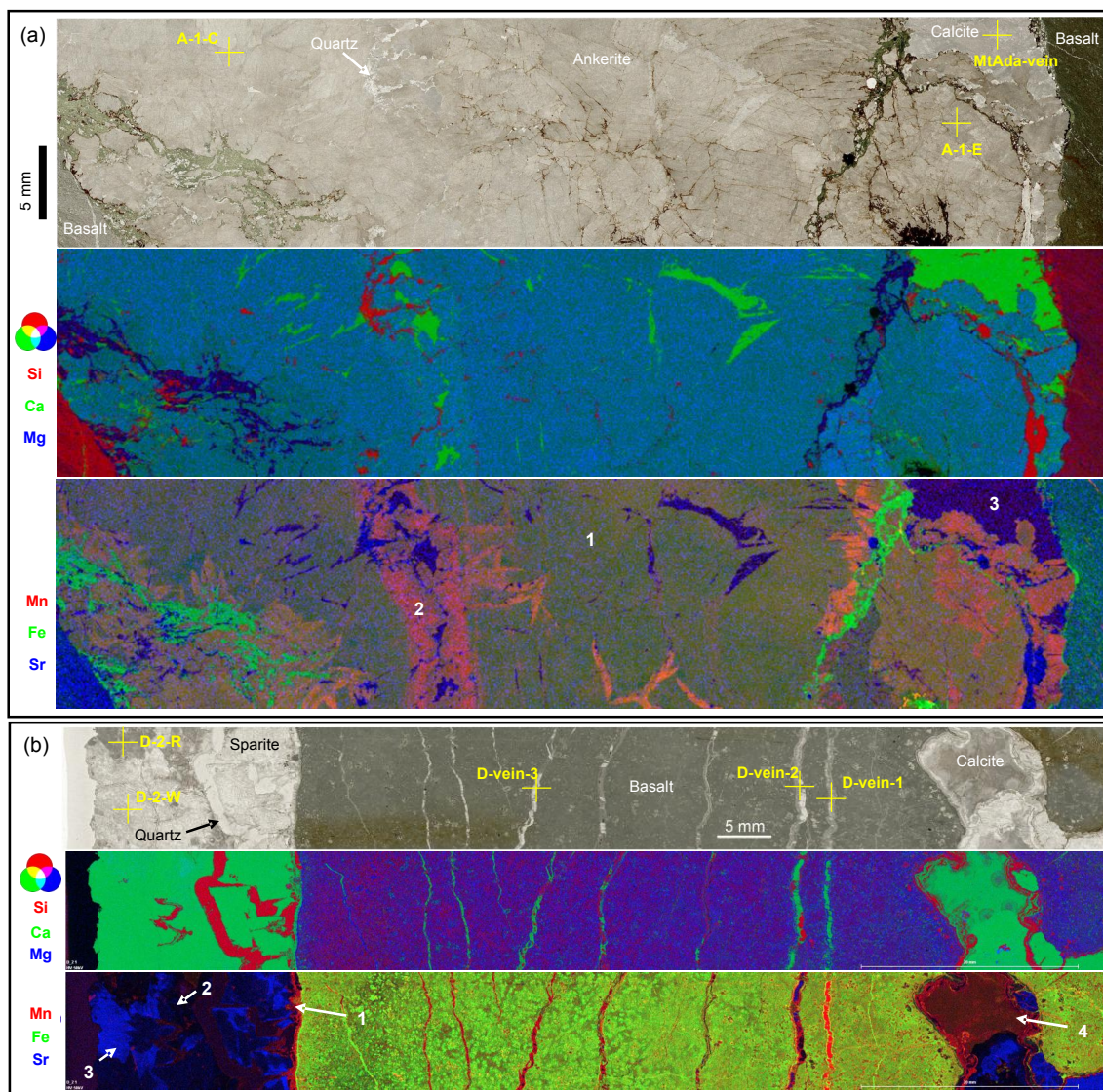
Figure 5: Thin section scan images (transmitted light) and false-colour overlapping images of elements of interstitial carbonates in (a) the Mount Ada Basalt and (b) the Dresser Formation. (a) Interstitial carbonate in the Mount Ada Basalt consists of blocky and massive ankerite with minor calcite overgrowth and infilling quartz, as evidenced by Fig. S4b and Si (red), Ca (green) and Mg (blue) distributions shown in false-colour overlapping images (middle panel in a). False-colour overlapping images of Mn (red), Fe (green) and Sr (blue) (lower panel in a) highlight the presence of Mn-enriched ankerite (close to metabasalt; number 2 in the figure), Mn-depleted calcite (in later vein; number 3), and ankerite with intermediate enrichments of Mn (distant to metabasalt; number 1). Mn-enriched ankerite might be influenced by later fluids as indicated by calcite and quartz. (b) Interstitial carbonates in the Dresser Formation includes precipitates enriched in Mn (first and fourth generations, shown in the figure by the numbers and arrows), depleted in Mn and Sr (second generation), as well as Mn-depleted but Sr-enriched precipitates (third generation).

Precipitates of the first and fourth generation seem identical to calcite occurring within parallel fractures of basalts, implying precipitation from similar fluids that derived from fluid-basalt reactions. The second and third generation are distinctive from the aforementioned generations, indicating a different origin of the later fluids. Yellow crosses mark the positions of subsamples analysed for stable oxygen and carbon isotopes (Table 1, Fig. S3). The images of each element are shown in Figs. S6, S7.

4.1.2 Primary carbonate phases

The primary mineral phase of interstitial carbonates is calcite. Acicular crystal-fans of calcite are only preserved in some samples from the Apex Basalt, but are reduced or absent in most other cases. The terminal tips of the acicular crystal-fans are partly recrystallized to sparitic calcite crystals (Fig. 4b). Microcrystalline ankerite is rarely observed at the basalt margin, mixing with microcrystalline quartz, chlorite, and anatase particles (~nm) (Figs. S2a, S4a). Minor chert locally infills the intercrystalline space of sparite and crystal-fan calcite. Primary carbonates occurring within basalts include blocky calcite in concentric syngenetic veins and fibrous isopachous calcite in tectonic fractures, often showing shear bending through dynamic crystallization (Fig. S2b, e).

Calcite is the dominant primary carbonate phase in all samples, which is in line with the spatially independent distributions of Ca, Mg and Si in the precipitates (Fig. 3b). However, distinct calcite phases show different contents of Mn, with acicular crystal-fan and fibrous isopachous precipitates being depleted in Mn relative to the associated intercrystalline calcites. Fe, Si and Mg are pervasive in basalt and fractures, which is due to the presence of chlorite group minerals (Fig. 5a).

4.1.3 Secondary carbonate facies

In many cases, primary interstitial calcite was affected by post-depositional alteration processes such as recrystallization and dolomitization. Recrystallization is widespread, involving the transformation of acicular crystal-fan calcite to inequigranular, blocky, massive, and sparry calcite (Fig. 4b–d). The recrystallized interstitial calcite is commonly cemented by quartz (Fig. 4e, g). In some samples, sparite exhibits a S-C fabric (Fig. 4f), indicative of deformation through dynamic metamorphism in a shear zone (Lister and Snoke, 1984). Noteworthy, sparite in sample D-2 from the Dresser Formation is rather associated with tectonic fractures than with basalt interspaces (Figs. 4d, S2 d-f; Xiang, 2023); therefore, it will be addressed as "fracture-filling calcite" in the following.

Carbonates from the Mount Ada Basalt underwent significant dolomitization, as indicated by abundant blocky and massive ankerite cemented by quartz (Fig. 4g). Rarely observed relict structures "floating" in ankerite evidence acicular crystal-fan calcite as precursor (Fig. S2c). The interstitial ankerite locally underwent recrystallization and neomorphism (Fig. 4h). Calcite veins locally cut the interstitial ankerite and the host basalt. Ankerite precipitates in those samples are commonly overgrown by calcite (Fig. 4g, i).

The recrystallized calcites are either Mn- or Sr-enriched (see Fig. 5), indicating at least two diagenetic fluids involved in recrystallization. The interstitial ankerite shows lower Sr enrichments than calcite cement in veins (Fig. 5a). Instead, it is enriched in Mn, which increasing abundances of Mn towards the basaltic parts. The Mn-enriched calcite is also observed in

fractures as fibrous cement. The fracture-filling calcite shows the highest Sr-enrichments of all analyzed carbonate phases (Fig. 5b).

4.1.4 $\delta^{13}C$ and $\delta^{18}O$ values of interstitial carbonates

255   The interstitial carbonates (including both, calcite and ankerite) show $\delta^{13}C$ values ranging from -2.37 to +0.99 ‰ (mean = 0.22 ± 0.98 ‰) and $\delta^{18}O$ values ranging from -19.81 to -14.34 ‰ (mean = -17.57 ± 1.51 ‰) (Table 1). The fracture-filling calcites exhibit $\delta^{13}C$ values ranging from 2.03 to 2.34 ‰ (mean = 2.19 ± 0.13 ‰) and $\delta^{18}O$ values ranging from -17.91 to -13.03 ‰ (mean = -15.70 ± 2.53 ‰) (Table 1). Carbonates in veins (see Figs. 3, 5) have the slightly lower $\delta^{13}C$ and $\delta^{18}O$ values than interstitial carbonates in the same samples (Table 1, Fig. S3).

260   **Table 1: Stable carbon and oxygen isotopic compositions of the early Archean carbonates**

Lithology	Formation	Age (Ma)	Sample ID	$\delta^{13}C_{VPDB}$ (‰)	s.d.	$\delta^{18}O_{VSMOW}$ (‰)	s.d.	$\delta^{18}O_{VPDB}$ (‰)
Interstitial Carb.	Euro Basalt	3350	E-1	0.21	0.03	11.08	0.05	-19.23
			E-2	0.99	0.03	10.78	0.05	-19.52
			E-3	-2.37	0.03	11.00	0.05	-19.31
	Apex Basalt	3460	A14673-1	0.62	0.03	13.65	0.05	-16.74
			A22-1	0.44	0.03	13.09	0.05	-17.29
			A22-2	0.69	0.03	13.67	0.05	-16.72
			ABAS-1	0.65	0.03	13.41	0.05	-16.97
			ABAS-1	0.77	0.03	14.63	0.05	-15.79
			Apex-1	0.25	0.03	12.79	0.05	-17.58
			Apex-2	0.04	0.03	12.66	0.05	-17.70
			Apex-3	0.21	0.03	13.00	0.05	-17.37
	Mt.Ada Basalt	3470	MtAda-1-C	0.83	0.00	12.21	0.03	-18.14
			MtAda-1-E	0.77	0.03	11.77	0.05	-18.57
			MtAda-2	0.52	0.03	14.36	0.03	-16.05
	Dresser Fm.	3480	D-1	0.97	0.03	14.46	0.05	-15.95
			D-3	0.63	0.03	10.49	0.05	-19.81
	North Star Basalt	3490	CP-1	-2.31	0.03	11.14	0.05	-19.17
			CP-2	0.01	0.03	16.12	0.05	-14.34
Fracture Carb.	Dresser Fm.	3480	D-2-IC-1	2.03	0.03	12.45	0.03	-17.91
			D-2-IC-2	2.17	0.03	16.43	0.03	-14.04

			D-2-R	2.34	0.03	12.54	0.05	-17.81
			D-2-W	2.20	0.03	17.47	0.05	-13.03
Veinlet Carb.	Apex Basalt	3460	A22-vein-1	0.12	0.03	13.50	0.05	-16.88
			A22-vein-2	-0.14	0.03	13.31	0.05	-17.07
			A22-vein-3	-0.02	0.03	13.29	0.05	-17.09
	Mt.Ada Basalt	3470	MtAda-1-vein	0.47	0.03	10.47	0.05	-19.82
	Dresser Fm.	3480	D-2-vein-1	-3.77	0.03	11.30	0.05	-19.02
			D-2-vein-2	-2.35	0.03	11.25	0.05	-19.06
			D-2-vein-3	-1.69	0.03	11.36	0.05	-18.96
Sed. Carb.	Euro Basalt	3350	E-4	1.88	0.00	15.24	0.03	-15.19
	Strelley Pool Fm.	3410	JR-Shaw-1	2.08		15.01		-15.42
		3410	JR-Shaw-2	2.52		15.24		-15.20
		3410	JR-Shaw-3	2.55		15.31		-15.13
	Dresser Fm.	3480	PDP	1.26	0.03	17.83	0.05	-12.69
			JR-TSU-1	2.24		17.53		-12.98
			JR-TSU-2	2.22		16.36		-14.11
			JR-TSU-3	2.17		16.71		-13.77
			JR-TSU-4	1.61		16.53		-13.95
			JR-TSU-5	2.24		17.68		-12.83
			JR-TSU-6	2.54		18.74		-11.80
			JR-TSU-7	2.42		18.30		-12.23
			JR-TSU-8	2.34	0.05	18.43	0.07	-12.10
			JR-TSU-9	1.21	0.05	27.10	0.07	-3.69
			JR-TSU-10	1.34	0.05	15.93	0.07	-14.53
			JR-TSU-11	1.61		15.82		-14.63
			JR-TSU-12	1.61		15.96		-14.50
			JR-TSU-13	1.49		15.74		-14.71
			JR-TSU-14	1.38		21.45		-9.17
			JR-TSU-15	1.10		22.60		-8.06
			JR-TSU-16	1.78		23.37		-7.31
			TSU	1.46	0.03	15.80	0.05	-14.66
Sed. Carb. DB			DB	-5.10	0.03	22.79	0.05	-7.88
			JR-Dress-1	-5.38		20.54		-10.05
			JR-Dress-2	-6.72		20.19		-10.40

			JR-Dress-3	-6.38		19.81		-10.77
			JR-Dress-4	-6.22		19.70		-10.87
			JR-Dress-5	-6.01		19.94		-10.64
			JR-Dress-6	-4.25		19.24		-11.32
			JR-Dress-7	-5.96	1.72	1.25	4.76	-28.77
			JR-Dress-8	-8.07	0.34	10.50	1.30	-19.79
			JR-Dress-9	-3.15	0.07	19.93	0.15	-10.65
Stromatolite	Strelley Pool Fm.	3410	Strelley	2.50	0.00	17.34	0.03	-13.16
			JR-Strell-1	2.46		13.92		-16.48
			JR-Strell-2	3.28		15.01		-15.42
			JR-Strell-3	3.38		14.84		-15.59
			JR-Strell-4	3.32	0.01	16.64	0.02	-13.84
			JR-Strell-5	2.69	0.01	15.74	0.03	-14.71
			JR-Strell-6	3.30	0.01	16.56	0.02	-13.92
			JR-Strell-7	3.33	0.01	16.66	0.02	-13.82
			JR-Strell-8	2.58	0.01	15.91	0.02	-14.55
			JR-Strell-9	3.21	0.01	16.68	0.03	-13.80
			JR-Strell-10	3.38	0.03	17.47	0.05	-13.04
			JR-Strell-11	3.15	0.01	16.56	0.02	-13.92
			JR-Strell-12	3.19	0.01	16.63	0.02	-13.84
			JR-Strell-13	3.14	0.02	16.66	0.03	-13.82
			JR-Strell-14	3.03	0.02	18.34	0.03	-12.19
			JR-Strell-15	3.05	0.01	16.77	0.02	-13.71
			JR-Strell-16	3.26	0.01	16.84	0.02	-13.65
			JR-Strell-17	3.31	0.01	16.70	0.03	-13.78
			JR-Strell-18	3.04	0.01	17.17	0.01	-13.33
Stromatolite?	Isua Supracrustal Belt	3700	IS12-1	2.35	0.08	18.80	0.11	-11.74
			IS12-2	1.21	0.08	19.69	0.11	-10.88
			IS12-3	1.18	0.08	19.57	0.11	-11.00
			IS12-4	1.11	0.08	19.59	0.11	-10.98
			IS12-5	1.18	0.13	19.36	0.18	-11.20
			IS12-6	1.27	0.08	19.01	0.11	-11.54
			IS12-7	0.45	0.08	16.85	0.11	-13.64
			JR-IS-1	0.74	0.08	19.30	0.11	-11.26
			JR-IS-2	0.98		19.23		-11.33
			IS-12	0.99	0.03	18.88	0.05	-11.66
			IS-12-C	1.03	0.03	19.44	0.03	-11.12
			IS-12-Q	0.78	0.03	19.27	0.03	-11.29

					s.d.		s.d.	
Metasomatic Carb.			**JR-IS9**	-2.11		11.46		-18.86
			IS9-1	-2.37	0.08	11.64	0.11	-18.69
			IS9-2	-1.84	0.08	11.16	0.11	-19.15
			IS9-3	-1.74	0.08	10.93	0.11	-19.38
			IS9-4	-1.93	0.08	11.49	0.11	-18.83
			IS9-5	-2.03	0.00	11.36	0.03	-18.96
Rhodochrosite	**Fig Tree Fm.**	**3260**	**Figtree-1**	-12.74		6.91		-23.28
			Figtree-2	-10.76		12.65		-17.71
			Figtree-3	-19.34		-4.93		-34.76
			Figtree-4	-12.12		5.90		-24.26
			Figtree-5	-18.23		-6.85		-36.62
			Figtree-6	-23.00		-12.32		-41.93
Carb. in barite	**Dresser Fm.**	**3480**	**JR-DressBart-1**	-18.14	0.20	9.37	0.50	-20.89
			JR-DressBart-2	-18.46	0.20	10.47	0.50	-19.82
			JR-DressBart-3	-11.37	0.20	11.32	0.50	-19.00
			JR-DressBart-4	-15.95	0.20	9.92	0.50	-20.36
			JR-DressBart-5	-11.07	0.20	10.81	0.50	-19.49
			JR-DressBart-6	-15.09	0.05	11.51	0.07	-18.82
			JR-DressBart-7	-11.81	0.10	12.06	0.30	-18.28
			JR-DressBart-8	-12.40	0.10	13.78	0.30	-16.61
			JR-DressBart-9	-9.79	0.10	12.85	0.30	-17.52
			JR-DressBart-10	-14.53	0.10	12.03	0.30	-18.31
			JR-DressBart-11	-11.20	0.20	12.30	0.50	-18.05
			JR-DressBart-12	-2.70	0.20	14.00	0.50	-16.40
			JR-DressBart-13	-10.83	0.10	12.54	0.30	-17.82
Carbonatite			**JR-C1**	-4.91		7.13		-23.07
			JR-C2	-5.84		7.13		-23.06
			JR-C3	-5.91		7.00		-23.19
			JR-C4	-3.29		18.35		-12.18

Note:

1. **$\delta^{18}O_{VPDB}=0.970017*\delta^{18}O_{VSMOW} -29.98$ (Coplen, 1988)**
2. **s.d. is the standard deviation calculated by multiple measurements of the in-house carbonate standard Solnhofen.**
3. **Abbreviations: Fm.- Formation , Mt.-Mount, Sed.-sedimentary, Carb. –carbonate;**
4. **The question mark in "Stromatolite (?)" indicates its controversial origin.**
5. **"Carb. in barite" refers to carbonate inclusions in bladed black barite.**

265

4.2 Sedimentary carbonates

4.2.1 Laminated micritic carbonates

Laminated micritic carbonate occurs in a ca. 5 m thick sedimentary succession (Fig. 6a, b) interbedded with pillow basalts of

270   the Dresser Formation (Fig. 2b). The micritic carbonate is predominantly brownish and finely bedded. The association with pillow basalts indicates an interval of generally quiet-water sedimentation, although the succession might preserve the oldest record of a tsunami event on Earth (Runge et al. 2022).
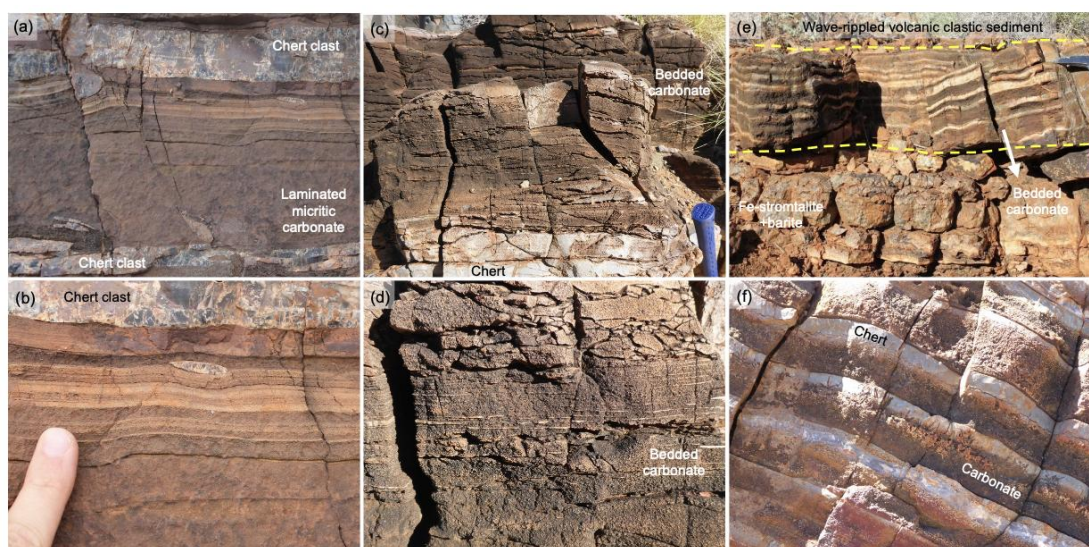
Figure 6: Outcrop photos of the bedded sedimentary carbonates from the North Pole Dome in the East Pilbara Terrane, Western

275   **Australia. (a, b) Laminated micritic sedimentary carbonate of Dresser Formation, the potential oldest reported tsunami deposit (Runge et al., 2022). (c, d) Finely bedded carbonate rock overlying the 3.35 Ga Euro Basalt. The shown bed is 10 cm thick. (e, f) Interlayered carbonate-chert beds (7 to 11 beds between the yellow dashed line) of Dresser Formation. This unit is overlain by wave rippled volcanic clastic sediment with remains of evaporitic minerals and organic films on top, while the underlying rock is bedded barite with sulfidic stromatolites atop. The length of hammer is ca. 40 cm.**

280   The laminated micritic carbonate consists of fine-grained carbonate crystals with abundant organic clots and flakes (Fig. 7a), and locally euhedral and subhedral carbonate rhombs that have a cloudy center and clear rim enveloped by organic matter (Fig. 7b). *In situ* geochemical mappings and Raman spectra (Fig. 7c, S8; Xiang, 2023) indicate that the carbonate crystals are Mn-enriched ankerite, while that the cloudy centers consist of organic matter. Calculated Raman-based temperatures (based on Lünsdorf et al., 2017) of ~ 300–350 °C agree well with the peak metamorphic temperatures of this region (Allwood et al.,

285   2006b; Hickman and Van Kranendonk, 2012a; Van Kranendonk et al., 2019a). The laminae are caused by changing crystal sizes and organic matter contents, with finer-grain sizes and higher organic matter contents resulting in darker colors. A similar bedded micritic carbonate is observed in samples from drilling core PDP2c (see Van Kranendonk et al., 2019b).
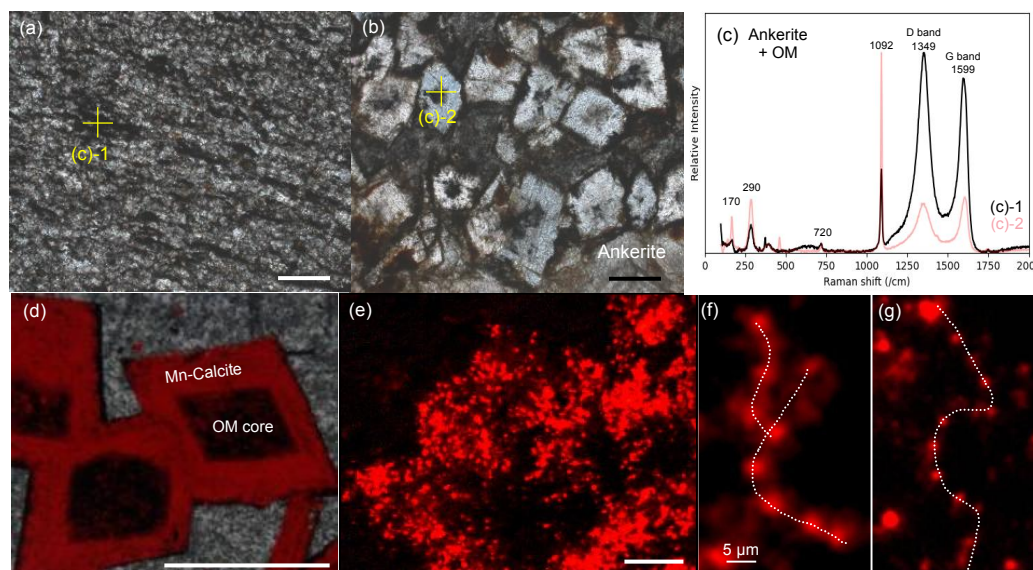
Figure 7: Spatial relationships between sedimentary carbonates and organic matter. (a) Interbed of the laminated micritic carbonate containing flakes and clots of organic material (OM). (b) Euhedral and subhedral carbonate rhombs, exhibiting organic matter in their cores and at their outer edges. (c) Raman spectra for spots in (a) and (c), supporting the presence of ankerite and organic matter. (d) Euhedral calcite rhombs with cores of organic matter are cemented by chert. (e) Close-up view of calcite rhombs showing Mn-enriched dolomite particles (kutnahorite?) within the calcite crust. (f, g) Arrangements of Mn-enriched dolomite particles that somewhat resemble kutnahorite formed by *Idiomarina loihiensis* strains (Rincón-Tomás et al., 2016). (a) and (b) were taken under plane-polarized light. The scale bar is 200 µm).

4.2.2 Bedded chert-carbonates

The bedded chert-carbonates are characterized by carbonate-chert couples and occur at the top of a chert layer from the Euro Basalt as well as in the Dresser Formation ("Euro bedded carbonate" and "Dresser bedded carbonate" in the following) (Fig. 6). The Dresser bedded carbonate consists of 9–11 carbonate-chert couplets with radiating crystal splays. Because of its distinct appearance, it was previously named "zebra rock" (Hickman and Van Kranendonk, 2012b; see Van Kranendonk et al. 2019b for a detailed description). Notably, it occurs between a unit consisting of sulfidic stromatolites and bladed barite below, and wave rippled volcanoclastic sediments above (Fig. 6e).

Individual carbonate-chert couplets consist of fining-upward successions of euhedral to subhedral carbonate rhombs in a chert matrix (Fig. 8a, b). In the Dresser bedded carbonate, carbonate rhombs are commonly calcite (Fig. S4c), and clusters of radiating calcite crystal splays occur at the base of each couplet (Figs. 6f, 8a). Some calcite rhombs have an organic core (Fig. 7d) and show a strong patchy Mn enrichment pattern under CL (Fig. 7e–g), somewhat similar to kutnahorite [Ca(Mn,Mg,Fe)(CO$_3$)$_2$] formed by modern *Idiomarina loihiensis* (ɣ-proteobacteria) (Rincón-Tomás et al., 2016). The euhedral to subhedral calcite rhombs and the highly porous chert matrix (Fig. 8b) indicate low compaction after deposition.

In the Euro bedded carbonate, organic matter is rare and only interbedded between carbonate crystals (ankerite; Fig. S4d, e).
310 Although the Euro bedded carbonate exhibits the repeated grading of dolomite rhombs in a chert matrix, pressure dissolution features associated with dolomite crystals and the nonporous microcrystalline chert matrix imply a stronger post-depositional compaction (Fig. S9a, b).
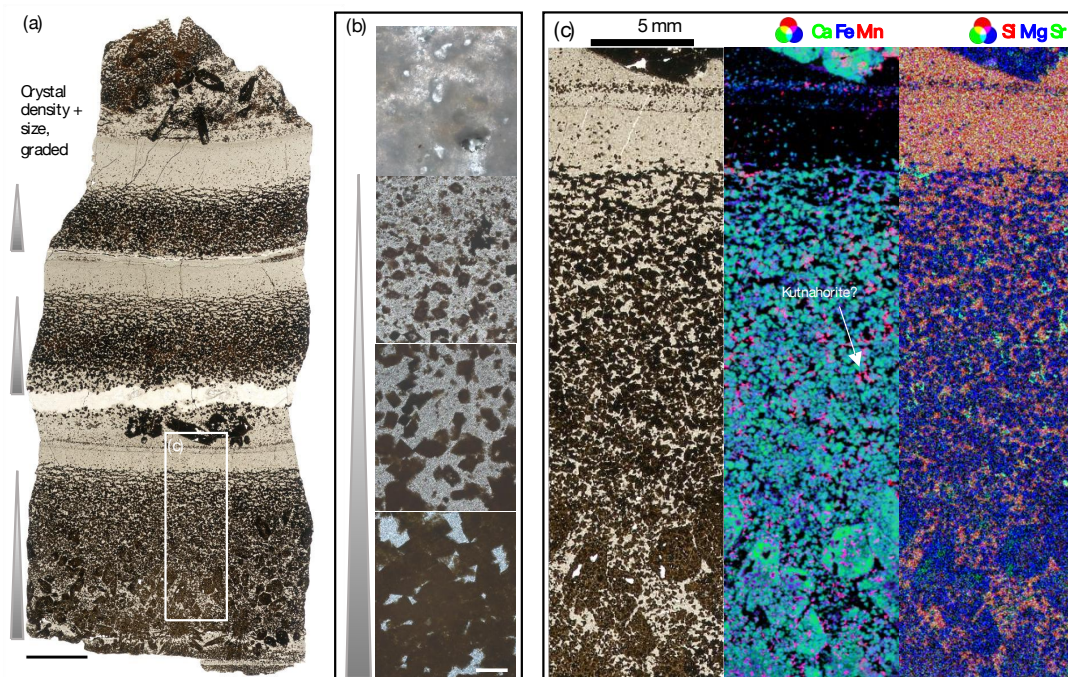
Figure 8: The bedded sedimentary carbonate-chert rock from Dresser Formation. (a) The scan image (transmitted light) of thin
315 **section shows repeated graded carbonate layers with the crystal size and density decreasing upwards. One layer is shown discontinuously in (b), that euhedral carbonates grade into the chert layer of high-porosity. The rectangle area is magnified in (c). (c) The false-colour overlapping images show that the Mn-dolomite particles distribute on the edge of calcite crystals. Scale bar in (a) is 10 mm and in (b) is 200 μm. The images of each element are shown in Fig. S10.**

In situ geochemical mappings reveal that the Dresser bedded carbonate predominantly consists of Fe-enriched calcite with
320 Mn-enriched dolomite particles along its edges (Fig. 8c), in agreement with the observed CL patterns. The Euro Basalt related bedded carbonate comprises Mn-enriched ankerite (Fig. S9).

4.2.3 $\delta^{13}C$ and $\delta^{18}O$ values of sedimentary carbonates

Laminated micritic carbonate and the Euro Basalt related bedded carbonate show $\delta^{13}C$ values between 1.10 and 2.55 ‰ (mean = 1.85 ± 0.48‰) and $\delta^{18}O$ values between -15.42 and -3.69 ‰ (mean = -12.75 ± 3.00 ‰) (Table 1). The Dresser
325 bedded carbonate, in contrast, exhibits the more negative $\delta^{13}C$ values ranging from -8.07 to -3.15 ‰ (mean = -5.72 ± 1.36 ‰) and $\delta^{18}O$ values ranging from -28.77 to -7.88 ‰ (mean = -13.11 ± 6.32 ‰) (Table 1).

4.3 Stromatolites

The stromatolitic carbonates were located from the second member of the Strelley Pool Formation. Stromatolite morphologies and arguments for biogenicity have been reported in detail elsewhere (Allwood et al., 2006a, 2007; Van Kranendonk et al. 2003; Van Kranendonk, 2011; Duda et al., 2016; Viehmann et al., 2020). Briefly, stromatolites show a high morphological diversity, ranging from coniform and finely laminated to large domical forms, and overly centimeter-sized carbonate fans (Fig. 9).
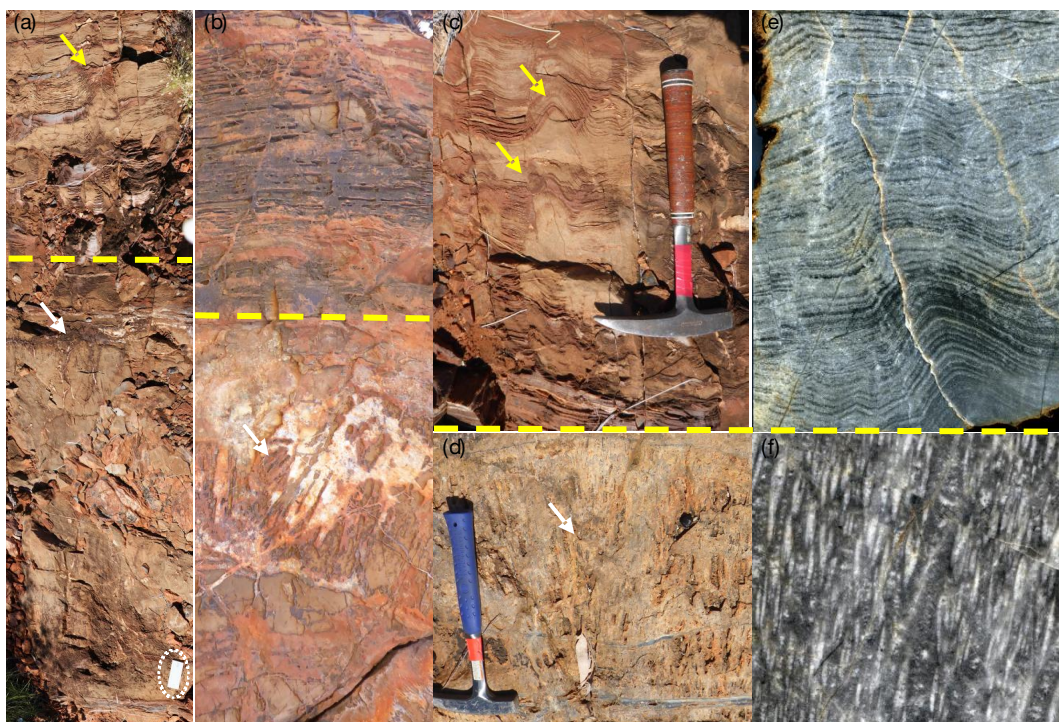
Figure 9: Photos of stromatolites from the Strelley Pool Formation near the Trendall site in the East Pilbara Terrane, Western Australia. The yellow dashed line marks the boundary between the upper unit with conical stromatolites (yellow arrow) and the lower unit with carbonate fans (white arrow). (a) Composite photo of the outcrop. The ruler (white dotted circle) is 15 cm in length. (b) Close-up view of an outcrop showing the layered stromatolite consisting of carbonate (weathered and partly absent) and chert (dark beds), atop the large carbonate fan on a chert matrix. (c, d) Close-up view of the conical stromatolites (c) and carbonate fans (d). (e, f) Cross-section views of samples corresponding to (c) and (d), respectively. The length of the brown and blue hammers in (c) and (d) are ~30 cm and ~40 cm, respectively.

The studied sample is a silicified coniform stromatolite with alternating laminae of equigranular anhedral dolomite that often preserves organic matter. The laminae margin contains euhedral dolomite overgrowth (Fig. S4f). Detailed cement stratigraphy involving CL microscopy indicate the presence of at least three dolomite generations (Fig. S11), in line with previous works (Allwood et al., 2009, 2010; Flannery et al., 2018).

345   The stromatolites show $\delta^{13}C$ values ranging from 2.46 to 3.38 ‰ (mean = 3.08 ± 0.30 ‰) and $\delta^{18}O$ values ranging from -16.48 to -12.19 ‰ (mean = -14.03 ± 0.98 ‰), consistent with data reported in Lindsay et al. (2005) and Flannery et al. (2018).

5 Discussion

5.1 Formation pathways of the EPT carbonates

350   The tectonic model of the EPT involves a volcanic plateau characterized by surface topographical changes, as indicated by pillow basalt successions and shallow water deposits (Smithies et al., 2003, 2005, 2007a, b; Van Kranendonk, 2006; Van Kranendonk et al, 2007a, b, 2019a). Our survey demonstrates that carbonates occur in very different EPT environments, ranging from deep marine settings to terrestrial ponds, which all have been differently influenced by hydrothermal processes.

5.1.1 Carbonate abiotically precipitated from hydrothermal fluids

355   Carbonates associated with Archean pillow basalts are well known from various localities worldwide (Roberts, 1987; Veizer, 1989a, b; Kitajima et al. 2001; Nakamura and Kato, 2004). Today, the formation of such carbonates is triggered by fluctuations in alkalinity, salinity and water temperature (Degens et al., 1984; Kempe, 1990; Reitner et al. 1995b; Flügel, 2010), i.e., the underlying processes are controlled by abiotic parameters. In modern settings, carbonates usually precipitate from low- to moderate-temperature hydrothermal fluids during the latest stage of seafloor alteration (Bach et al., 2001, 2003,

360   2011; Coogan and Gillis, 2013); as a consequence, they tend to be more abundant in older crusts (Gillis et al., 2001; Heft et al., 2008; Coogan and Gillis, 2013). The precipitation of Ca-Mg-Fe carbonates and formation of silica-bearing fluids linked to basalt-fluid interactions has also been demonstrated by experimental work and numerical simulations (~22 to 350 °C) (Gysi and Stefánsson, 2011; Gudbrandsson et al., 2011; Stockmann et al., 2011; Galeczka et al., 2013a, b, 2014; McGrail et al., 2017; Menefee et al., 2018; Wolff-Boenisch and Galeczka, 2018; Xiong et al., 2018; Voigt et al., 2018).

365   There is no evidence for a potential biological influence on the formation of EPT basalt-associated carbonates as for instance organic remains. At the same time, precipitation of these carbonates could have been abiotically triggered by infiltration of CO_2-enriched seawater and/or basalt-water interactions under hydrothermal conditions, which result in a higher alkalinity and higher cation concentrations (Fig. 10). Indeed, fracture-filling calcite shows the lowest $^{87}Sr/^{86}Sr$ ratio (0.700596) and REE+Y pattern that is considered typical of Archean seawater (Xiang, 2023), indicating the percolation of seawater-derived

370   CO_2-rich fluids through basaltic crust 3.5 Ga ago (Kitajima et al. 2001; Nakamura and Kato, 2002; Yamamoto et al., 2004). In this light, $\delta^{13}C$ signatures of fracture-filling calcites (2.18 ± 0.13 ‰ on average; Fig. 11) may reflect Archean seawater, while $\delta^{13}C$ signatures of interstitial carbonates (0.22 ± 0.98 ‰ on average; Fig. 11) indicate admixture of hydrothermally derived mantle-derived carbon ($\delta^{13}C$ of -5 to -6 ‰; Degens et al. 1984, Hayes and Waldbauer 2006). This is reflected in the common lower $\delta^{13}C$ values of veinlet carbonates than the interstitial carbonates (Fig. S3).

375
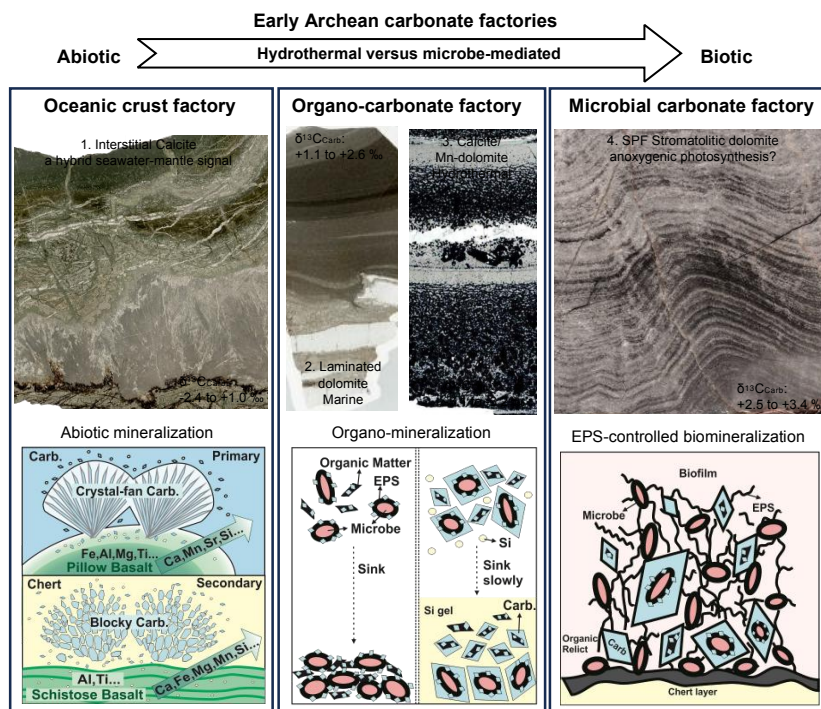
Figure 10: The lithological features and formation pathways of the three carbonate factories in the early Archean, including an oceanic crust factory, an organo-carbonate factory and a microbial carbonate factory. Carbon precipitation in the oceanic crust factory is an abiotic and inorganic process driven by seawater-basalt interaction, which produce hydrothermal fluids with high carbonate alkalinity and high cation concentrations. Carbonate

380 **precipitation in the organo-carbonate factory is linked to organic macromolecules (i.e., organo-mineralization). Carbonate precipitation in the microbial carbonate factory occurs through EPS-controlled biomineralization, with anoxygenic photoautotrophs being a likely source of the EPS (adapted from Reitner et al., 2001). (Abbreviations in the figure: "Carb./ Carb"- carbonate; "EPS"- extracellular polymeric substances)**
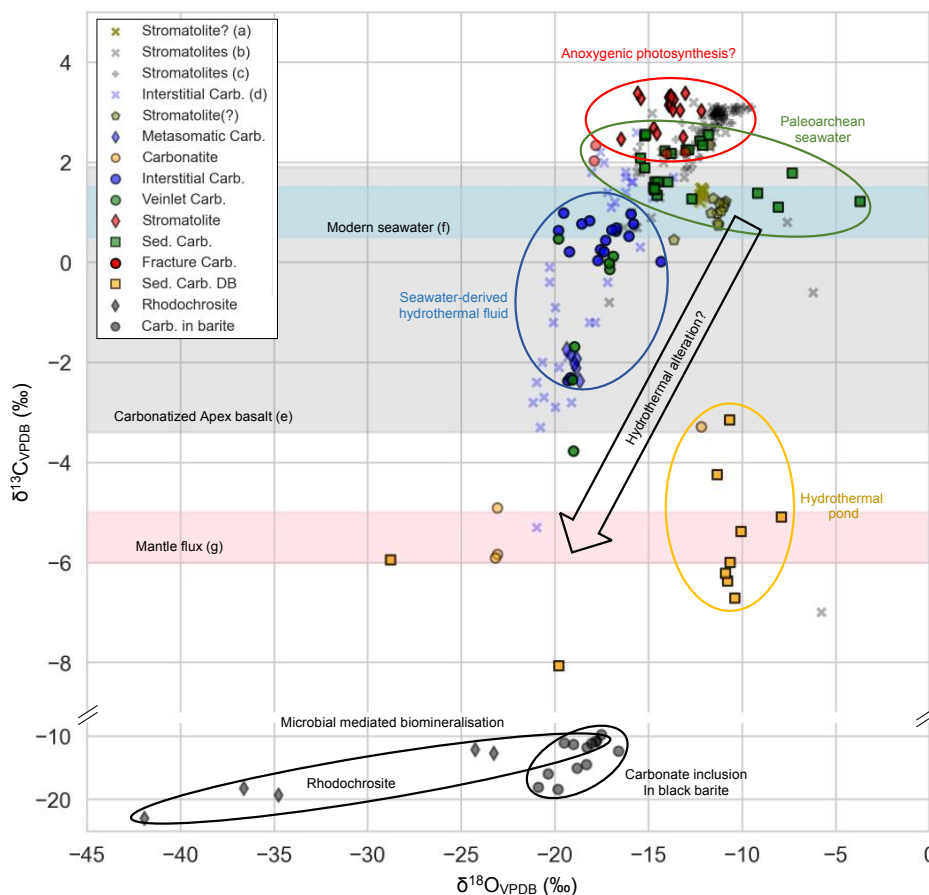
385 **Figure 11: Stable carbon and oxygen isotopic (δ^{13}C, δ^{18}O) compositions of early Archean carbonates (Carb.). In tendency, δ^{13}C and δ^{18}O values decrease from the stromatolite through marine sedimentary carbonate (Sed. Carb.) to interstitial carbonate, possibly reflecting increasing admixture of mantle-derived carbon. Own data (square, circle, diamond, and pentagon symbols) are given in Table 1. Reference data (including cross and plus symbols) from (a) Nutman et al. (2016), (b) Lindsay et al. (2005), (c) Flannery et al. (2018), (d) Shibuya et al. (2012), (e) Nakamura and Kato (2004), (f) Kroopnick (1980) and Tan (1988), (g) Degens et al. (1984), and Hayes and Waldbauer (2006). Note that "Carb. in barite" indicates carbonate inclusions in black barites from the ~3.5 Ga Dresser Formation (Western Australia), and that question marks in sample labels highlight the controversial biogenicity of the material.**

The mixture of different fluids is also supported by ^{87}Sr/^{86}Sr ratios of primary interstitial calcite associated with the Apex basalt (0.703094 ± 0.000979), laying between those of early Archean seawater and Apex pillow basalt (0.700596 and 0.706337 ± 0.000954, respectively; Xiang, 2023). On the other hand, the precipitation of calcite in vesicles and veins of basalts, as well as the formation of acicular calcite crystal-fans growing at pillow margins (Fig. 3a), could have been driven by an elevated alkalinity and higher Ca levels, which derived from hydrothermal basalt-water interactions. The observed

blocky and massive interstitial calcite or ankerite (Figs. 4, 5) probably resulted from recrystallization and dolomitization of primary calcite precipitates, driven by Mg-, Fe-, Al-, Si-, and Mn-enriched fluids deriving from hydrothermal chlorite

400   breakdown in the basalts (Fig. 3). In summary, carbonates associated with pillowed basalts are inferred to have precipitated abiotically on and below the seafloor (Fig. 12)
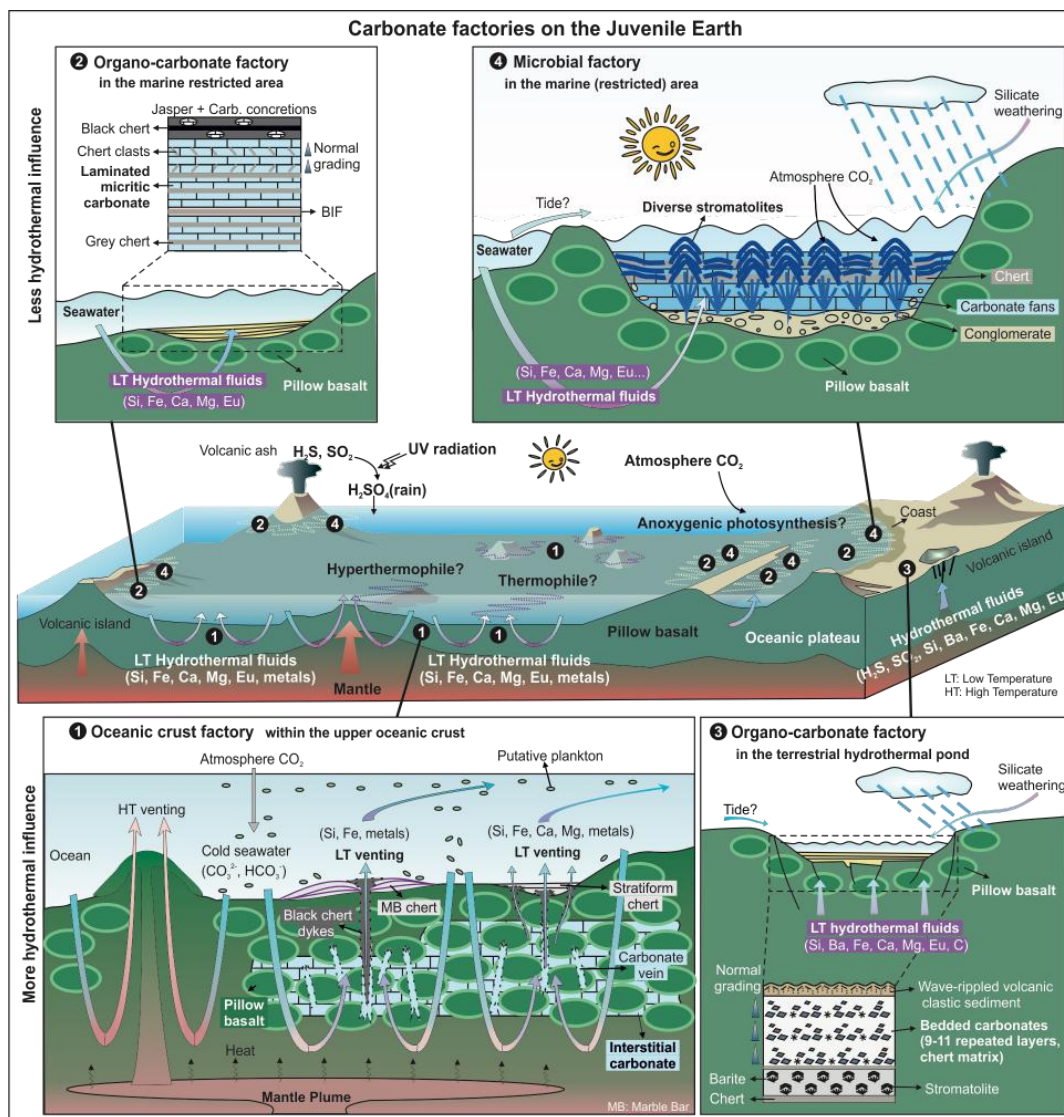
Figure 12: The possible localities of the three early Archean carbonate factories (adapted from Nisbet and Sleep, 2001; Runge et al., 2022). The oceanic crust factory commonly occurs in deeper marine environments within the upper oceanic crust (number 1).

405   **The organo-carbonate factory may operate in diverse environments where organic matter (biotic and/or abiotic) is abundant and fluids are supersaturated in Ca²⁺ and CO₂, and which are intermittently influenced by hydrothermal fluids (number 2 and 3). The**

microbial factory likely forms in photic, relatively restricted, shallow marine environments like lagoons on the slope or platform, with minor detritus and rare hydrothermal inputs (number 4).

5.1.2 Bedded sedimentary carbonates – a product of organo-mineralization

410 EPT bedded sedimentary carbonate rocks preserve abundant organic remains, for instance occurring as dispersed flakes and clots within micrite (Fig. 7), perhaps indicating a genetic relationship. Organic matrices and compounds inherited from living organisms may retain mineralizing properties (Dé farge and Trichet, 1995; Trichet and Dé farge, 1995). To distinguish minerals formed through mineralization linked to organic matrices and compounds from those whose formation is induced by living organisms, the terms "organomineral" and "organo-mineralization" were introduced at the 7th

415 International Symposium on Biomineralization in 1995 and further developed in the following decade (Dé farge and Trichet, 1995; Reitner et al., 1995b, 1997; Arp et al., 1999, 2001, 2003; Neuweiler et al., 1999; Riding, 2000; Pratt, 2001; Reitner, 2004; Gautret and Trichet, 2005), before being finally consummated in following studies (Perry et al., 2007, 2009; Dé farge et al., 2009; Altermann et al., 2009).

Fine-grained carbonates such as micritic calcite or dolomite are typical products of organo-mineralization. Indeed, micrite

420 can form autochthonously (i.e., "automicrite"), involving Ca-binding by aspartic acid- and glutamic acid-rich (briefly, Asp- and Glu-) proteinous macromolecules and negatively charged polysaccharids initiating carbonate crystal nucleation (Reitner et al. 1995a, b, c; Reitner and Neuweiler, 1995; Trichet and Dé farge, 1995). It is consequently termed "organomicrite", which is a distinct subset of automicrite (Reitner et al., 1995b). Organomicrites are widespread in Phanerozoic carbonate depositional systems, particularly important in microbial mats and biofilms (Reitner et al., 1995a, b, c; Riding, 2000;

425 Schlager, 2000 2003; Reitner and Thiel, 2011; Reijmer, 2021), as well as in the SPF stromatolites. However, it is important to highlight that organo-mineralization is not restricted to organic matter from biological sources (Dé farge et al., 2009); in fact, laboratory experiments indicated that abiotic organic matter as e.g. from the Murchison CM2 meteorite can also mediate carbonate precipitation (Reitner, 2004).

Organomicrites are abundant in some EPT facies. The precipitation and sedimentation of organomicrites result in the finely

430 laminated carbonate deposits (Figs. 7a, 10). However, carbonate precipitation was more complicated in case of fine-graded, bedded chert-carbonates (Figs. 7b-d, 10). In this case, organomicrites can serve as new nucleation centers for the development of euhedral carbonate rhombs. Under low-energy conditions, the fine-grained carbonate crystals precipitate slowly, displaying pronounced normal grading (Figs. 8b, 10). On the other hand, occurrence of Fe/Mn-enriched carbonates and the chert matrix is indicative of involvement of Si-bearing hydrothermal fluids in this process (Fig. 8). Hydrothermal

435 fluids provided significant alkaline metals and silicon. Silicon precipitated as opal-A, a soluble hydrated amorphous silica phase that deposited as siliceous gel, which was converted to chert during diagenesis (Ledevin, 2019). The cyclical repeat of this process resulted in the formation of bedded sedimentary carbonate (Fig. 8a).

$\delta^{13}C$ signatures of some EPT bedded sedimentary carbonates except the Dresser bedded carbonates (1.85 ± 0.48‰ on average) are generally in line with a formation in marine environments. At the same time, $\delta^{13}C$ values of the Dresser bedded

440 carbonates are relatively depleted (-5.72 ±1.36 ‰ on average), which in good accordance with $\delta^{13}C$ signatures of carbonatites (-4.99 ± 1.22 ‰ on average) (Fig.11), indicating hydrothermal admixture of mantle-derived carbon. The occurrence of rippled volcanic clastic sediments atop (Fig. 6e) indicates a shallow water environment. The clusters of radiating calcite crystals at the base of each carbonate-chert layer (Figs. 6f, 8a), which were initially proposed to be gypsum or aragonite (Runnegar et al., 2001; Van Kranendonk et al., 2008; Otálora et al., 2018), are likely indicative of evaporitic

445 conditions. The $\delta^{13}C$ values and field relationships imply that the Dresser bedded carbonates perhaps formed in a terrestrial hydrothermal pond with intermittent inputs, akin to recently identified hot spring deposits (Djokic et al., 2017, 2021). Hence, bedded sedimentary carbonates formed across a spectrum of environments, ranging from shallow marine to terrestrial settings.

5.1.3 Stromatolites formed through microbial activity

450 Stromatolites, first described by Kalkowsky (1908), are defined as laminated benthic microbial deposits (Hofmann, 1973; Buick et al., 1981; Riding, 1999; Flügel, 2010). Although the biogenicity of early Archean stromatolites is commonly controversial, the biogenicity of stromatolites from the Dresser Formation and the SPF has been widely accepted (Lambert et al. 1978; Van Kranendonk 2006, 2007; Allwood et al. 2006a, 2007, 2009; Marshall et al. 2007; Wacey, 2010; Bontognali et al., 2012; Duda et al. 2016; Flannery et al. 2018). Carbonates associated with SPF stromatolites are thought to be related to

455 microbial processes (Van Kranendonk 2007, 2011; Lepot, 2020).

Stromatolites typically form through biologically induced or controlled mineralization within microbial mats or biofilms, commonly related to physicochemical gradients and/or organic substances providing nucleation sites for mineral precipitation (Reitner et al., 2000). In any case, extracellular polymeric substances (EPS) secreted by microorganisms, amongst others to cope with environmental stressors, play a key-role in mineralization (Decho, 2011; see in Fig. 10). Certain

460 functional groups of organic substances in the EPS (e.g. Asp- and Glu-rich macromolecules) efficiently bind and sequester divalent cations such as Ca^{2+} and Mg^{2+}, thereby inhibiting their complexation with carbonate anions and subsequent precipitation (Reitner et al. 1995a, b, c). This process is similar to organo-mineralization, which indeed involves in the formation of stromatolites. Dé farge (2011) ascribed the distinction between organo-mineralization and biological induced biomineralization to be a space- and time-remoted function of nucleating organic substrates in organo-mineralization.

465 However, in case of EPS-controlled biomineralization, carbonate nucleation and growth are extracellular processes, which are triggered by the metabolic activity of microorganisms and related changes in the immediate environment (Heim, 2011).

EPS-controlled biomineralization might have played a role in case of the SPF stromatolites, as supported by $\delta^{13}C$ signatures of carbonates. More specifically, $\delta^{13}C$ values of carbonates from SPF stromatolites (3.08 ± 0.30 ‰ on average) are heavier than those of the interstitial carbonates and the sedimentary carbonates (~0.22 -1.85 ‰ on average; Fig. 11). This difference

470 is well in line with a sequestration of ^{12}C by photoautotrophic microorganisms in the microbial mats, resulting in an enrichment of ^{13}C in the environment and, consequently, in the carbonate. Additionally, the positive $\delta^{13}C$ values of the SPF stromatolites are distinctive to those of rhodochrosite from the Fig Tree Group and of carbonate inclusions in black barites of

the Dresser Formation (-16.03 ± 4.86 ‰ and -12.56 ± 4.10 ‰ on average, respectively; Fig. 11), which are assumed to precipitate from microbial biomineralization and hydrothermal carbon. Flannery et al. (2018) reported a substantial $\delta^{13}C_{org}$

475 fractionation in SPF stromatolites and fan-like carbonates (similar to the materials investigated herein), ranging from -29 to -45 ‰. It is documented to be compelling evidence for the coexistence of autotrophic possibly anoxygenic photosynthesis or predominantly heterotrophic metabolisms alongside the Calvin-Benson-Bassham (CBB) cycle (Flannery et al., 2018). Anoxygenic phototrophs appear to be plausible candidate microorganisms, given that they likely appeared about 3.8–3.4 billion years ago (Awramik, 1992; Brasier et al., 2006; Moore et al., 2017; Lepot, 2020). Taken together, carbonates

480 associated with SPF stromatolites precipitated in shallow marine environments, perhaps lagoon-like, relatively restricted basin (see Fig.12).

5.2 Early Archean carbonate factories – implications

Depending on the formation mechanisms, the EPT carbonates can be assigned to three carbonate factories: (i) an oceanic crust factory, (ii) an organo-carbonate factory, and (iii) a microbial carbonate factory. The formation pathways and

485 depositional environments are summarized in Table 2. The oceanic crust factory includes abiotically formed carbonates such as Mn- or Sr-enriched calcite and ankerite that are associated with pillow basalts. Precipitation was linked CO_2-rich seawater-derived hydrothermal fluids with a high alkalinity and high cation loads. The organo-carbonate factory is dominated by authigenic carbonates formed through taphonomy-controlled organo-mineralization (i.e. organomicrites). Importantly, and in contrast to the microbial carbonate factory, the involved organic matter can be of either biological or

490 abiotic origin. The microbial carbonate factory is somewhat similar to the organo-carbonate factory, but specifically refers to EPS-controlled carbonate precipitation, that is, mineralization of biologically derived organic substances. However, as in case of the organo-carbonate factory, organomicrite is formed as a typical product. Given that most of these carbonates formed in shallow-water environments under anoxic conditions, anoxygenic phototrophs appear a plausible source of biological organic matter, but this remains to be tested in future studies.

495 In case of all three carbonate factories, hydrothermal fluids play a key role in the formation and preservation of carbonate precipitates. The precipitation of carbonates might for instance be directly driven by basalt-alteration, or rather indirectly by providing a nutrient source for EPS-forming microorganisms. Preservation of carbonates is commonly promoted by hydrothermally driven silicification in the environment or during early diagenesis, which is well known for carbonaceous materials in early Archean rocks (Glikson et al., 2008; Alleon et al., 2016; Duda et al., 2016, 2018; van Zuilen, 2019;

500 Hickman-Lewis, 2019; Ledevin, 2019; Lepot, 2020). Our study shows that such processes are also critical for the preservation of very delicate features in carbonates, allowing for the identification of precipitates formed in the three carbonate factories.

The two major carbon reservoirs on modern Earth are biological organic matter and carbonates (Gislason and Oelkers, 2014; Hoefs, 2018; Shields, 2019). Hence, all three discussed carbonate factories would have provided significant carbon sinks

505 during the early Archean, likely exerting a significant influence on the global carbon cycle. This is particularly important

since carbon removal through terrestrial silicate weathering, constituting a major sink in the younger history of our planet, must have been much less significant in the early Archean due to the rare presence of continental crust during that time (Taylor and McLennan, 1981; Arndt, 1999; Flament et al., 2008; Cawood et al., 2013; Korenaga, 2021).

Table 2: Features of the three carbonate factories in the early Archean

Features	Oceanic crust factory	Organo-carbonate factory	Microbial carbonate factory
Primary lithology	Acicular crystal-fan calcite	Organomicrite, calcite or ankerite crystals of various size, on a chert matrix	Laminated dolomite layers cemented by chert
Secondary lithology	Sparite, blocky, massive calcite and ankerite	Anhedral dolomite crystals showing compaction and pressure dissolution	Several generations of dolomites, including prismatic dolomite cement
Organic Materials (OM)	Absent	Abundant	Abundant
Origins of OM	-	Abiotic to biogenic	Biogenic
Hydrothermal inputs	Dominant	Common	Rare
Main origins of carbonate	Inorganic precipitation from seawater or seawater-derived hydrothermal fluids	Taphonomy-controlled organo-mineralization	EPS-controlled microbial mineralization
Evaporite minerals	Absent	Common to rare	Common to rare
Silicon in fluid	Source/sink	Sink	Sink
Siliciclastic sediments	Absent	Common	Common
Depositional setting	Deeper marine within the upper ocean basaltic crust	Diverse, shallow ocean to terrestrial hydrothermal pond	Photic shallow marine slope/ platform

510

Among the three early Archean carbonate factories, the oceanic crust factory might have been the most substantial carbon sink. Carbonatized greenstones are widespread in the early Archean (Kitajima et al., 2001; Nakamura and Kato, 2002, 2004; Anhaeusser, 2014; Kasting, 2019; Nutman et al., 2019a; herein). Based on studies of carbonatized pillow basalts in the Pilbara Craton, the CO_2 flux from the ocean to the oceanic crust is estimated to be $> 3.8 \times 10^{13}$ and 1.5×10^{14} mol per year in

515   the early and middle Archean, respectively (Nakamura and Kato, 2004; Shibuya et al., 2012), which is 1–2 orders of magnitude higher than present-day fluxes (1.5–2.4×10^{12} mol per year: Alt and Teagle, 1999). Consequently, carbonatization of oceanic crust likely played a significant role in the early Archean global carbon cycle (Nakamura and Kato, 2004; Shibuya et al., 2012; Coogan and Gillis, 2013).

6 Conclusion

520 Paleoarchean rocks in the Pilbara Craton (Western Australia) contain carbonates of various origin. Three carbonate factories are recognized: (i) an oceanic crust factory, (ii) an organo-carbonate factory, and (iii) a microbial carbonate factory. The oceanic crust factory is characterized by carbonates associated with pillowed basalts, which precipitated abiotically on and within basaltic oceanic crust from CO_2-enriched seawater and seawater-derived alkaline hydrothermal fluids. The organo-carbonate factory encompasses carbonate that formed via taphonomy-controlled organo-mineralization linked to organic

525 macromolecules (either biotic or abiotic). The microbial carbonate factory includes carbonates formed through mineralization controlled by microbial extracellular polymeric substances (EPS). In case of all three carbonates factories, hydrothermal fluids seem to play also an important role in the formation and preservation of mineral precipitates. Our study demonstrates the great value of Paleoarchean carbonates for the reconstruction of geobiological processes. At the same time, our findings highlight that Paleoarchean carbonates might have been major carbon sinks at the time of formation, modulating

530 the carbon cycle and, hence, climate variability on early Earth.

Data availability. The data are presented in the manuscript; and can be requested from the corresponding author.

Author contribution. Xiang, Reitner and Duda designed the framework and methodology of this study. Reitner and van Zuilen contributed to the fieldwork, sample and data collections. Pack was involved in data interpretation. Xiang is responsible for data collection, analysis and interpretation, and drafting the manuscript. All co-authors have been involved in

535 the critical revisions of the manuscript, and approved the final manuscript for submission.

Competing interests. The authors declare that they have no conflict of interest.

Acknowledgements. We thank A. Hackmann and W. Dröse for sample preparation, B. Schmidt, J. Schönig for their help with Raman spectroscopy and micro-XRF, A. Kronz for carrying out EPMA mappings, and T. Di Rocco, D. Kohl and T. Wasselin for stable isotope measurements, all geoscience faculty of University of Göttingen. M. van Kranendonk (Curtain

540 University Perth, Western Australia) as well as F. Myers and G. Myers acknowledged for their assistance in the field and providing rock material. A. Hickman (Geological Survey of Western Australia) and A. Hofmann (University of Johannesburg, South Africa) thanked for providing information of the Pilbara Craton and the Barberton Greenstone Belt, respectively. The core library of the Geological Survey of Western Australia, is acknowledged for permission to sample drill core materials from the Pilbara region (approval for P954, 1014, 1091). This study was financially supported by the China

545 Council Scholarship (CSC), the German Research Foundation (DFG) priority program (SPP)1833 "Building a Habitable Earth" (RE 665/42-2; DU 1450/3-1, DU 1450/3-2; TH 713/13-2), and the Göttingen Academy of Sciences and Humanities in Lower Saxony.

References

550 Addadi, L., Weiner, S.: Interactions between acidic proteins and crystals: stereochemical requirements in biomineralization, Proceedings of the National Academy of Sciences, 82, 4110-4114, 1985.

Addadi, L., Raz, S., and Weiner, S.: Taking advantage of disorder: amorphous calcium carbonate and its roles in biomineralization, Advanced Materials, 15, 959–970, https://doi.org/10.1002/adma.200300381, 2003.

Alleon, J., Bernard, S., Le Guillou, C., Daval, D., Skouri-Panet, F., Pont, S., Delbes, L., and Robert, F.: Early entombment 555 within silica minimizes the molecular degradation of microorganisms during advanced diagenesis, Chemical Geology, 437, 98–108, 2016.

Allwood, A. C., Walter, M. R., Kamber, B. S., Marshall, C. P., and Burch, I. W.: Stromatolite reef from the Early Archaean era of Australia, Nature, 441, 714–718, 2006a.

Allwood, A. C., Walter, M. R. , & Marshall, C. P.: Raman spectroscopy reveals thermal palaeoenvironments of c.3.5 560 billion-year-old organic matter. Vibrational Spectroscopy, 41, 190-197, 2006b.

Allwood, A. C., Walter, M. R., Burch, I. W., and Kamber, B. S.: 3.43 billion-year-old stromatolite reef from the Pilbara Craton of Western Australia: ecosystem-scale insights to early life on Earth, Precambrian Research, 158, 198–227, 2007.

Allwood, A. C., Grotzinger, J. P., Knoll, A. H., Burch, I. W., Anderson, M. S., Coleman, M. L., and Kanik, I.: Controls on development and diversity of Early Archean stromatolites, Proceedings of the National Academy of Sciences, 106, 9548– 565 9555, 2009.

Allwood, A. C., Kamber, B. S., Walter, M. R., Burch, I. W., and Kanik, I.: Trace elements record depositional history of an Early Archean stromatolitic carbonate platform, Chemical Geology, 270, 148–163, 2010.

Allwood, A. C., Rosing, M. T., Flannery, D. T., Hurowitz, J. A., and Heirwegh, C. M.: Reassessing evidence of life in 3,700-million-year-old rocks of Greenland, Nature, 563, 241–244, 2018.

570 Alt, J. C. and Teagle, D. A.: The uptake of carbon during alteration of ocean crust, Geochimica et Cosmochimica Acta, 63, 1527–1535, 1999.

Altermann, W., Bö hmer, C., Gitter, F., Heimann, F., Heller, I., Lä uchli, B., and Putz, C.: Defining Biominerals and Organominerals: Direct And Indirect Indicators Of Life. Perry et al., Sedimentary Geology, 201,157-179, Sedimentary Geology, 213, 150–151, https://doi.org/10.1016/j.sedgeo.2008.04.001, 2009.

575 Andersen, T. and Taylor, P. N.: Pb isotope geochemistry of the Fen carbonatite complex, SE Norway: Age and petrogenetic implications, Geochimica et Cosmochimica Acta, 52, 209–215, https://doi.org/10.1016/0016-7037(88)90069-5, 1988.

Anhaeusser, C. R.: Archaean greenstone belts and associated granitic rocks–a review, Journal of African Earth Sciences, 100, 684–732, 2014.

Arndt, N.: Why was flood volcanism on submerged continental platforms so common in the Precambrian?, Precambrian
580 Research, 97, 155–164, 1999.

Arp, G., Reimer, A., and Reitner, J.: Calcification in cyanobacterial biofilms of alkaline salt lakes, European Journal of
Phycology, 34, 393—403, 1999.

Arp, G., Reimer, A., and Reitner, J.: Photosynthesis-induced biofilm calcification and calcium concentrations in Phanerozoic
oceans, Science, 292, 1701–1704, 2001.

585 Arp, G., Reimer, A., and Reitner, J.: Microbialite formation in seawater of increased alkalinity, Satonda Crater Lake,
Indonesia, Journal of Sedimentary Research, 73, 105—-127, 2003.

Awramik, S. M.: The oldest records of photosynthesis, Photosynthesis research, 33, 75–89,
https://doi.org/10.1007/BF00039172, 1992.

Bach, W., Alt, J. C., Niu, Y., Humphris, S. E., Erzinger, J., and Dick, H. J.: The geochemical consequences of late-stage
590 low-grade alteration of lower ocean crust at the SW Indian Ridge: Results from ODP Hole 735B (Leg 176), Geochimica et
Cosmochimica Acta, 65, 3267–3287, 2001.

Bach, W., Peucker-Ehrenbrink, B., Hart, S. R., and Blusztajn, J. S.: Geochemistry of hydrothermally altered oceanic crust:
DSDP/ODP Hole 504B–Implications for seawater-crust exchange budgets and Sr-and Pb-isotopic evolution of the mantle,
Geochemistry, Geophysics, Geosystems, 4, 2003.

595 Bach, W., Rosner, M., Jö ns, N., Rausch, S., Robinson, L. F., Paulick, H., and Erzinger, J.: Carbonate veins trace seawater
circulation during exhumation and uplift of mantle rock: Results from ODP Leg 209, Earth and Planetary Science Letters,
311, 242–252, 2011.

Bontognali, T. R., Sessions, A. L., Allwood, A. C., Fischer, W. W., Grotzinger, J. P., Summons, R. E., and Eiler, J. M.:
Sulfur isotopes of organic matter preserved in 3.45-billion-year-old stromatolites reveal microbial metabolism, Proceedings
600 of the National Academy of Sciences, 109, 15 146–15 151, 2012.

Bower, D., Steele, A., Fries, M., Green, O., and Lindsay, J.: Raman imaging spectroscopy of a putative microfossil from the
3.46 Ga Apex chert: Insights from quartz grain orientation, Astrobiology, 16, 169–180, 2016.

Brasier, M. D., Green, O. R., Jephcoat, A. P., Kleppe, A. K., Van Kranendonk, M. J., Lindsay, J. F., Steele, A., and
Grassineau, N. V.: Questioning the evidence for Earth's oldest fossils, Nature, 416, 76–81, 2002.

605 Brasier, M., Green, O., Lindsay, J., and Steele, A.: Earth's Oldest (3.5 Ga) Fossils and theEarly Eden Hypothesis':
Questioning the Evidence, Origins of Life and Evolution of the Biosphere, 34, 257–269, 2004.

Brasier, M. D., Green, O. R., Lindsay, J. F., McLoughlin, N., Steele, A., and Stoakes, C.: Critical testing of Earth's oldest
putative fossil assemblage from the 3.5 Ga Apex chert, Chinaman Creek, Western Australia, Precambrian Research, 140,
55–102, 2005.

610 Brasier, M., McLoughlin, N., Green, O., and Wacey, D.: A fresh look at the fossil evidence for early Archaean cellular life,
Philosophical Transactions of the Royal Society B: Biological Sciences, 361, 887–902, 2006.

Brasier, M. D., Antcliffe, J., Saunders, M., and Wacey, D.: Changing the picture of Earth's earliest fossils (3.5–1.9 Ga) with new approaches and new discoveries, Proceedings of the National Academy of Sciences, 112, 4859–4864, 2015.

Buick, R., Dunlop, J., and Groves, D.: Stromatolite recognition in ancient rocks: an appraisal of irregularly laminated structures in an Early Archaean chert-barite unit from North Pole, Western Australia, Alcheringa, 5, 161–181, https://doi.org/10.1080/03115518108566999, 1981.

Byerly, G. R., Lowe, D. R., Wooden, J. L., and Xie, X.: An Archean impact layer from the Pilbara and Kaapvaal cratons, Science, 297, 1325–1327, 2002.

Cantine, M. D., Knoll, A. H., and Bergmann, K. D.: Carbonates before skeletons: A database approach, Earth-Science Reviews, 201, 103 065, https://doi.org/10.1016/j.earscirev.2019.103065, 2020.

Cawood, P. A., Hawkesworth, C., and Dhuime, B.: The continental record and the generation of continental crust, Geological Society of America Bulletin, 125, 14–32, 2013.

Coogan, L. A. and Gillis, K. M.: Evidence that low-temperature oceanic hydrothermal systems play an important role in the silicate-carbonate weathering cycle and long-term climate regulation, Geochemistry, Geophysics, Geosystems, 14, 1771–1786, 2013.

Copper, P.: Reef development at the Frasnian/Famennian mass extinction boundary, Palaeogeography, Palaeoclimatology, Palaeoecology, 181, 27–65, 2002.

Decho, A. W.: Extracellular polymeric substances (EPS), in: Encyclopedia of Geobiology, edited by Reitner, J. and Thiel, V., pp. 359–361, Springer, Berlin, 2011.

Dé farge, C. and Trichet, J.: From biominerals to 'organominerals': The example of the modern lacustrine calcareous stromatolites from Polynesian atolls, in: Bulletin de l'Institut Océ anographique de Monaco, n◦ spé c. 14, edited by Allemand, D. and Cuif, J., vol. 2, pp. 265—271, Proc. 7th Int. Symp. Biomineralization, 1995.

Dé farge, C., Gautret, P., Reitner, J., and Trichet, J.: Defining Organominerals: Comment On 'defining Biominerals And Organominerals: Direct And Indirect Indicators Of Life' By Perry et al.(2007, Sedimentary Geology, 201,157-179), Sedimentary Geology, 213, 152–155, https://doi.org/10.1016/J.SEDGEO.2008.04.002, 2009.

Degens, E. T., Wong, H.-K., Kempe, S., and Kurtman, F.: A geological study of Lake Van, eastern Turkey, Geologische Rundschau, 73, 701–734, https://doi.org/10.1007/BF01824978, 1984.

Delarue, F., Robert, F., Derenne, S., Tartè se, R., Jauvion, C., Bernard, S., Pont, S., Gonzalez-Cano, A., Duhamel, R., and Sugitani, K.: Out of rock: A new look at the morphological and geochemical preservation of microfossils from the 3.46 Gyr-old Strelley Pool Formation, Precambrian Research, 336, 105 472, 2020.

Djokic, T., Van Kranendonk, M. J., Campbell, K. A., Walter, M. R., and Ward, C. R.: Earliest signs of life on land preserved in ca. 3.5 Ga hot spring deposits, Nature communications, 8, 15 263, 2017.

Djokic, T., Van Kranendonk, M. J., Campbell, K. A., Havig, J. R., Walter, M. R., and Guido, D. M.: A reconstructed subaerial hot spring field in the 3.5 billion-year-old Dresser Formation, North Pole Dome, Pilbara Craton, Western Australia, Astrobiology, 21, 1–38, 2021.

Duda, J.-P., Van Kranendonk, M. J., Thiel, V., Ionescu, D., Strauss, H., Schä fer, N., and Reitner, J.: A rare glimpse of Paleoarchean life: Geobiology of an exceptionally preserved microbial mat facies from the 3.4 Ga Strelley Pool Formation, Western Australia, PLoS One, 11, e0147 629, 2016.

Duda, J.-P., Thiel, V., Bauersachs, T., Mißbach, H., Reinhardt, M., Schä fer, N., Van Kranendonk, M. J., and Reitner, J.:
650   Ideas and perspectives: hydrothermally driven redistribution and sequestration of early Archaean biomass–the "hydrothermal pump hypothesis", Biogeosciences, 15, 1535–1548, 2018.

Escoffier, N., Perolo, P., Lambert, T., Rü egg, J., Odermatt, D., Adatte, T., Vennemann, T., and Perga, M.-E.: Whiting Events in a Large Peri-Alpine Lake: Evidence of a Catchment-Scale Process, Journal of Geophysical Research: Biogeosciences, 127, e2022JG006 823, 2022.

655   Flament, N., Coltice, N., and Rey, P. F.: A case for late-Archaean continental emergence from thermal evolution models and hypsometry, Earth and Planetary Science Letters, 275, 326–336, 2008.

Flannery, D. T., Allwood, A. C., Summons, R. E., Williford, K. H., Abbey, W., Matys, E. D., and Ferralis, N.: Spatially-resolved isotopic study of carbon trapped in 3.43 Ga Strelley Pool Formation stromatolites, Geochimica et Cosmochimica Acta, 223, 21–35, 2018.

660   Flü gel, E.: Microfacies of carbonate rocks: analysis, interpretation and application, vol. 976, Springer, 2nd., 2010.

French, K. L., Hallmann, C., Hope, J. M., Schoon, P. L., Zumberge, J. A., Hoshino, Y., Peters, C. A., George, S. C., Love, G. D., Brocks, J. J., et al.: Reappraisal of hydrocarbon biomarkers in Archean rocks, Proceedings of the National Academy of Sciences, 112, 5915–5920, https://doi.org/10.1073/pnas.1419563112, 2015.

Galeczka, I., Wolff-Boenisch, D., and Gislason, S.: Experimental studies of basalt-H_2O-CO_2 interaction with a high pressure
665   column flow reactor: the mobility of metals, Energy Procedia, 37, 5823–5833, https://doi.org/10.1016/j.egypro.2013.06.505, 2013a.

Galeczka, I., Wolff-Boenisch, D., Jonsson, T., Sigfusson, B., Stefansson, A., and Gislason, S.: A novel high pressure column flow   reactor   for   experimental   studies   of CO_2 mineral   storage,   Applied   Geochemistry,   30,   91–104, https://doi.org/10.1016/j.apgeochem.2012.08.010, 2013b.

670   Galeczka, I., Wolff-Boenisch, D., Oelkers, E. H., and Gislason, S. R.: An experimental study of basaltic glass–H_2O–CO_2 interaction at 22 and 50 °C: Implications for subsurface storage of CO_2, Geochimica et Cosmochimica Acta, 126, 123–145, https://doi.org/10.1016/j.gca.2013.10.044, 2014.

Gardiner, N. J., Wacey, D., Kirkland, C. L., Johnson, T. E., and Jeon, H.: Zircon U–Pb, Lu–Hf and O isotopes from the 3414 Ma Strelley Pool Formation, East Pilbara Terrane, and the Palaeoarchaean emergence of a cryptic cratonic core, Precambrian
675   Research, 321, 64–84, https://doi.org/10.1016/j.precamres.2018.11.023, 2019.

Gautret, P. and Trichet, J.: Automicrites in modern cyanobacterial stromatolitic deposits of Rangiroa, Tuamotu Archipelago, French Polynesia: Biochemical parameters underlaying their formation, Sedimentary Geology, 178, 55–73, https://doi.org/10.1016/j.sedgeo.2005.03.012, 2005.

Geological Survey of Western Australia, cartographer, Western Australia. Department of Mines and Petroleum, and

680   Exploration Incentive Scheme (W.A.): 1:100 000 GIS Pilbara 2013 update / Geological Survey of Western Australia, 2013.

Germs, G. J.: New shelly fossils from Nama Group, south west Africa, American Journal of Science, 272, 752–761, https://doi.org/10.2475/ajs.272.8.752, 1972.

Gillis, K. M., Muehlenbachs, K., Stewart, M., Gleeson, T., and Karson, J.: Fluid flow patterns in fast spreading East Pacific Rise crust exposed at Hess Deep, Journal of Geophysical Research: Solid Earth, 106, 26 311–26 329,

685   https://doi.org/10.1029/2000JB000038, 2001.

Gislason, S. R. and Oelkers, E. H.: Carbon storage in basalt, Science, 344, 373–374, https://doi.org/10.1126/science.1250828, 2014.

Glikson, M., Duck, L. J., Golding, S. D., Hofmann, A., Bolhar, R., Webb, R., Baiano, J. C., and Sly, L. I.: Microbial remains in some earliest Earth rocks: comparison with a potential modern analogue, Precambrian Research, 164, 187–200,

690   https://doi.org/10.1016/j.precamres.2008.05.002, 2008.

Grant, S.: Shell structure and distribution of *Cloudina*, a potential index fossil for the terminal Proterozoic, American Journal of Science, 290, 261–294, 1990.

Grotzinger, J. P. and Knoll, A. H.: Anomalous carbonate precipitates: is the Precambrian the key to the Permian?, Palaios, 10, 578–596, https://doi.org/10.2307/3515096, 1995.

695   Grotzinger, J. P. and Knoll, A. H.: Stromatolites in Precambrian carbonates: evolutionary mileposts or environmental dipsticks?, Annual review of earth and planetary sciences, 27, 313–358, https://doi.org/10.1146/annurev.earth.27.1.313, 1999.

Grotzinger, J. P. and James, N. P.: Precambrian carbonates: evolution of understanding, in: Carbonate Sedimentation and Diagenesis in the Evolving Precambrian World, SEPM Society for Sedimentary Geology, https://doi.org/10-2110/pec.00.67, 2000.

700   Gudbrandsson, S., Wolff-Boenisch, D., Gislason, S. R., and Oelkers, E. H.: An experimental study of crystalline basalt dissolution from $2 \leq pH \leq 11$ and temperatures from 5 to 75 C, Geochimica et Cosmochimica Acta, 75, 5496–5509, https://doi.org/10.1016/j.gca.2011.06.035, 2011.

Gysi, A. P. and Stefá nsson, A.: CO_2–water–basalt interaction. Numerical simulation of low temperature CO_2 sequestration into basalts, Geochimica et Cosmochimica Acta, 75, 4728–4751, https://doi.org/10.1016/j.gca.2011.05.037, 2011.

705   Hayes, J. M. and Waldbauer, J. R.: The carbon cycle and associated redox processes through time, Philosophical Transactions of the Royal Society B: Biological Sciences, 361, 931–950, https://doi.org/10.1098/rstb.2006.1840, 2006.

Heft, K. L., Gillis, K. M., Pollock, M. A., Karson, J. A., and Klein, E. M.: Role of upwelling hydrothermal fluids in the development of alteration patterns at fast spreading ridges: Evidence from the sheeted dike complex at Pito Deep, Geochemistry, Geophysics, Geosystems, 9, https://doi.org/10.1029/2007GC001926, 2008.

710   Heim, C.: Microbial biomineralization, in: Encyclopedia of Geobiology, edited by Reitner, J. and Thiel, V., pp. 586–591, Springer, Berlin, 2011.

Heinrichs, T.: Lithostratigraphische Untersuchungen in der Fig Tree Gruppe des Barberton Greenstone Belt zwischen Umsoli und Lomati (Sü dafrika), Göttinger Arbeiten zur Geologie und Paläontologie, 22, 1-118, 1980

Hickman, A. H. and Van Kranendonk, M.: A Billion Years of Earth History: A Geological Transect Through the Pilbara Craton and the Mount Bruce Supergroup-a Field Guide to Accompany 34th IGC Excursion WA-2, Geological Survey of Western Australia, Record 2012/10, 2012a.

Hickman, A. H. and Van Kranendonk, M. J.: Early Earth evolution: evidence from the 3.5–1.8 Ga geological history of the Pilbara region of Western Australia, Episodes Journal of International Geoscience, 35, 283–297, https://doi.org/10.18814/epiiugs/2012/v35i1/028, 2012b.

Hickman, A., Van Kranendonk, M., and Grey, K.: State Geoheritage Reserve R50149 (Trendall Reserve), North Pole, Pilbara Craton, Western Australia — geology and evidence for early Archean life. Geological Survey of Western Australia Record 2011/10, 2011.

Hickman-Lewis, K., Westall, F., and Cavalazzi, B.: Trace of early life in the Barberton greenstone belt, in: Earth's Oldest Rocks, edited by Van Kranendonk, M., Bennett, V., and Hoffmann, E., pp. 1029–1058, Elsevier, https://hal.science/hal-03041208, 2019.

Higgins, J. A., Fischer, W., and Schrag, D.: Oxygenation of the ocean and sediments: consequences for the seafloor carbonate factory, Earth and Planetary Science Letters, 284, 25–33, https://doi.org/10.1016/j.epsl.2009.03.039, 2009.

Hoefs, J.: Stable isotope geochemistry, Springer International Publishing AG, part of Springer Nature, 8th ed., 2018.

Hofmann, H.: Stromatolites: characteristics and utility, Earth-Science Reviews, 9, 339–373, https://doi.org/10.1016/0012-8252(73)90002-0, 1973.

Hofmann, A. and Harris, C.: Silica alteration zones in the Barberton greenstone belt: a window into subseafloor processes 3.5–3.3 Ga ago, Chemical Geology, 257, 221–239, https://doi.org/10.1016/j.chemgeo.2008.09.015, 2008.

Hofmann, H., Grey, K., Hickman, A., and Thorpe, R.: Origin of 3.45 Ga coniform stromatolites in Warrawoona group, Western Australia, Geological Society of America Bulletin, 111, 1256–1262, https://doi.org/10.1130/0016-7606(1999)111<1256:OOGCSI>2.3.CO;2, 1999.

Kalkowsky, E.: Oolith und Stromatolith im norddeutschen Buntsandstein., Zeitschrift der deutschen geologischen Gesellschaft, pp. 68–125, 1908.

Kasting, J. F.: Early Earth Atmosphere and Oceans, in: Earth's Oldest Rocks, edited by Van Kranendonk, M.J., B. V. H. J., pp. 49–61, Elsevier, 2019.

Kato, Y. and Nakamura, K.: Origin and global tectonic significance of Early Archean cherts from the Marble Bar greenstone belt, Pilbara Craton, Western Australia, Precambrian Research, 125, 191–243, https://doi.org/10.1016/S0301-9268(03)00043-3, 2003.

Kempe, S.: Alkalinity: the link between anaerobic basins and shallow water carbonates?, Naturwissenschaften, 77, 426–427, 1990.

745   Kitajima, K., Maruyama, S., Utsunomiya, S., and Liou, J.: Seafloor hydrothermal alteration at an Archaean mid-ocean ridge, Journal of Metamorphic Geology, 19, 583–599, https://doi.org/10.1046/j.0263-4929.2001.00330.x, 2001.

Knoll, A. H., Bambach, R. K., Payne, J. L., Pruss, S., and Fischer, W. W.: Paleophysiology and end-Permian mass extinction, Earth and Planetary Science Letters, 256, 295–313, https://doi.org/10.1016/j.epsl.2007.02.018, 2007.

Komiya, T., Maruyama, S., Hirata, T., and Yurimoto, H.: Petrology and geochemistry of MORB and OIB in the mid-
750   Archean North Pole region, Pilbara craton, Western Australia: implications for the composition and temperature of the upper mantle at 3.5 Ga, International Geology Review, 44, 988–1016, https://doi.org/10.2747/0020-6814.44.11.988, 2002.

Korenaga, J.: Was there land on the early Earth?, Life, 11, 1142, https://doi.org/10.3390/life11111142, 2021.

Kozawa, T., Sugitani, K., Oehler, D. Z., House, C. H., Saito, I., Watanabe, T., and Gotoh, T.: Early Archean planktonic mode of life: Implications from fluid dynamics of lenticular microfossils, Geobiology, 17, 113–126,
755   https://doi.org/10.1111/gbi.12319, 2019.

Kraml, M., Pik, R., Rahn, M., Selbekk, R., Carignan, J., and Keller, J.: A new multi-mineral age reference material for $^{40}Ar/^{39}Ar$, (U-Th)/He and fission track dating methods: the Limberg t3 tuff, Geostandards and Geoanalytical Research, 30, 73–86, https://doi.org/10.1111/j.1751- 908X.2006.tb00914.x, 2006.

Lambert, I., Donnelly, T., Dunlop, J., Groves, and DI: Stable isotopic compositions of early Archaean sulphate deposits of
760   probable evaporitic and volcanogenic origins, Nature, 276, 808–811, https://doi.org/10.1038/276808a0, 1978.

Ledevin, M.: Archean cherts: Formation processes and paleoenvironments, in: Earth's Oldest Rocks, edited by Van Kranendonk, M., Bennett, V., and Hoffmann, J., pp. 913–944, Elsevier, 2019.

Lees, A. and Buller, A. T.: Modern temperate-water and warm-water shelf carbonate sediments contrasted, Marine Geology, 13, M67–M73, https://doi.org/10.1016/0025-3227 (72)90011-4, 1972.

765   Lepot, K., Williford, K. H., Ushikubo, T., Sugitani, K., Mimura, K., Spicuzza, M. J., and Valley, J. W.: Texture-specific isotopic compositions in 3.4 Gyr old organic matter support selective preservation in cell-like structures, Geochimica et Cosmochimica Acta, 112, 66–86, https://doi.org/10.1016/j.gca.2013.03.004, 2013.

Lepot, K.: Signatures of early microbial life from the Archean (4 to 2.5 Ga) eon, Earth-Science Reviews, 209, 103296, https://doi.org/10.1016/j.earscirev.2020.103296, 2020.

770   Lindsay, J., Brasier, M., McLoughlin, N., Green, O., Fogel, M., Steele, A., and Mertzman, S.: The problem of deep carbon— an Archean paradox, Precambrian Research, 143, 1–22, https://doi.org/10.1016/j.precamres.2005.09.003, 2005.

Lister, G. and Snoke, A.: SC mylonites, Journal of Structural Geology, 6, 617–638, https://doi.org/10.1016/0191-8141(84)90001-4, 1984.

Lowe, D. R.: Stromatolites 3,400-Myr old from the Archean of Western Australia, Nature, 284, 441–443, 1980.

775   Lowe, D. R.: Restricted shallow-water sedimentation of Early Archean stromatolitic and evaporitic strata of the Strelley Pool Chert, Pilbara Block, Western Australia, Precambrian Research, 19, 239–283, https://doi.org/10.1016/0301-9268(83)90016-5, 1983.

Lu, Y., Paulmann, C., Mihailova, B., Malcherek, T., Birgel, D., Correa, M. L., Lin, Z., Lu, L., Milker, Y., and Peckmann, J.: Fibrous dolomite formation at a Miocene methane seep may reflect Neoproterozoic aragonite-dolomite sea conditions, Communications Earth Environment, 4, 2023.

Lü nsdorf, N. K., Dunkl, I., Schmidt, B. C., Rantitsch, G., and von Eynatten, H.: Towards a higher comparability of geothermometric data obtained by Raman spectroscopy of carbonaceous material. Part 2: A revised geothermometer, Geostandards and Geoanalytical Research, 41, 593–612, https://doi.org/10.1111/ggr.12178, 2017.

Marshall, C. P., Love, G. D., Snape, C. E., Hill, A. C., Allwood, A. C., Walter, M. R., Van Kranendonk, M. J., Bowden, S. A., Sylva, S. P., and Summons, R. E.: Structural characterization of kerogen in 3.4 Ga Archaean cherts from the Pilbara Craton, Western Australia, Precambrian Research, 155, 1–23, https://doi.org/10.1016/j.precamres.2006.12.014, 2007.

McCollom, T. M. and Seewald, J. S.: Carbon isotope composition of organic compounds produced by abiotic synthesis under hydrothermal conditions, Earth and Planetary Science Letters, 243, 74–84, https://doi.org/10.1016/j.epsl.2006.01.027, 2006.

McCollom, T. M., Ritter, G., and Simoneit, B. R.: Lipid synthesis under hydrothermal conditions by Fischer-Tropsch-type reactions, Origins of Life and Evolution of the Biosphere, 29, 153–166, https://doi.org/10.1023/A:1006592502746, 1999.

McGrail, B. P., Schaef, H. T., Spane, F. A., Cliff, J. B., Qafoku, O., Horner, J. A., Thompson, C. J., Owen, A. T., and Sullivan, C. E.: Field validation of supercritical CO2 reactivity with basalts, Environmental Science & Technology Letters, 4, 6–10, https://doi.org/10.1021/acs.estlett.6b00387, 2017.

McKeegan, K. D., Kudryavtsev, A. B., and Schopf, J. W.: Raman and ion microscopic imagery of graphitic inclusions in apatite from older than 3830 Ma Akilia supracrustal rocks, west Greenland, Geology, 35, 591–594, https://doi.org/10.1130/G23465A.1, 2007.

McNaughton, N., Compston, W., and Barley, M.: Constraints on the age of the Warrawoona Group, eastern Pilbara block, Western Australia, Precambrian Research, 60, 69–98, https://doi.org/10.1016/0301-9268(93)90045-4, 1993.

Menefee, A. H., Giammar, D. E., and Ellis, B. R.: Permanent CO_2 trapping through localized and chemical gradient-driven basalt carbona- tion, Environmental science & technology, 52, 8954–8964, https://doi.org/10.1021/acs.est.8b01814, 2018.

Mojzsis, S. J., Arrhenius, G., McKeegan, K., Harrison, T., Nutman, A., and Friend, C.: Evidence for life on Earth before 3,800 million years ago, Nature, 384, 55–59, https://doi.org/10.1038/384055a0, 1996.

Moore, E. K., Jelen, B. I., Giovannelli, D., Raanan, H., and Falkowski, P. G.: Metal availability and the expanding network of microbial metabolisms in the Archaean eon, Nature Geoscience, 10, 629–636, https://doi.org/10.1038/ngeo3006, 2017.

Morag, N., Williford, K. H., Kitajima, K., Philippot, P., Van Kranendonk, M. J., Lepot, K., Thomazo, C., and Valley, J. W.: Microstructure- specific carbon isotopic signatures of organic matter from 3.5 Ga cherts of the Pilbara Craton support a biologic origin, Precambrian Research, 275, 429–449, https://doi.org/10.1016/j.precamres.2016.01.014, 2016.

Nakamura, K. and Kato, Y.: Carbonate minerals in the Warrawoona Group, Pilbara Craton: Implications for continental crust, life, and global carbon cycle in the Early Archean, Resource Geology, 52, 91–100, https://doi.org/10.1111/j.1751-3928.2002.tb00122.x, 2002.

Nakamura, K. and Kato, Y.: Carbonatization of oceanic crust by the seafloor hydrothermal activity and its significance as a CO_2 sink in the Early Archean, Geochimica et Cosmochimica Acta, 68, 4595–4618, https://doi.org/10.1016/j.gca.2004.05.023, 2004.

815 Neuweiler, F. and Reitner, J.: Initially indurated structures of fine-grained calcium carbonate formed in place (automicrite), Biomineralization 93: Abstract volume of the 7th International Symposium on Biomineralization: Musé e Océ anographique, Monaco, p. 159, 1993.

Neuweiler, F., Gautret, P., Thiel, V., Lange, R., Michaelis, W., and Reitner, J.: Petrology of Lower Cretaceous carbonate mud mounds (Albian, N. Spain): insights into organomineralic deposits of the geological record, Sedimentology, 46, 837—

820 859, https://doi.org/10.1046/j.1365- 3091.1999.00255.x, 1999.

Nijman, W. and de Vries, S. T.: Early Archaean crustal collapse structures and sedimentary basin dynamics, in: The Precambrian Earth: Tempos and Events, edited by Eriksson, P., Altermann, W., Nelson, D., Mueller, W., and Catuneau, O., pp. 139–154, Elsevier, Amsterdam, 2004.

Nisbet, E. and Sleep, N.: The habitat and nature of early life, Nature, 409, 1083–1091, https://doi.org/10.1038/35059210,

825 2001.

Nutman, A. P., Bennett, V. C., Friend, C. R., Van Kranendonk, M. J., and Chivas, A. R.: Rapid emergence of life shown by discovery of 3,700-million-year-old microbial structures, Nature, 537, 535–538, https://doi.org/10.1038/nature19355, 2016.

Nutman, A. P., Friend, C. R., Bennett, V. C., Van Kranendonk, M., and Chivas, A. R.: Reconstruction of a 3700 Ma transgressive marine environment from Isua (Greenland): Sedimentology, stratigraphy and geochemical signatures, Lithos,

830 346, 105164, https://doi.org/10.1016/j.lithos.2019.105164, 2019a.

Nutman, A. P., Bennett, V. C., Friend, C. R., Van Kranendonk, M. J., Rothacker, L., and Chivas, A. R.: Cross-examining Earth's oldest stromatolites: Seeing through the effects of heterogeneous deformation, metamorphism and metasomatism affecting Isua (Greenland) 3700 Ma sedimentary rocks, Precambrian Research, 331, 105 347, https://doi.org/10.1016/j.precamres.2019.105347, 2019b.

835 Nutman, A. P., Bennett, V. C., Friend, C. R., and Van Kranendonk, M. J.: In support of rare relict 3700 Ma stromatolites from Isua (Green- land), Earth and Planetary Science Letters, 562, 116 850, https://doi.org/10.1016/j.epsl.2021.116850, 2021.

Oehler, D. Z., Robert, F., Walter, M. R., Sugitani, K., Allwood, A., Meibom, A., Mostefaoui, S., Selo, M., Thomen, A., and Gibson, E. K.: NanoSIMS: insights to biogenicity and syngeneity of Archaean carbonaceous structures, Precambrian Research, 173, 70–78, https://doi.org/10.1016/j.precamres.2009.01.001, 2009.

840 Ohtomo, Y., Kakegawa, T., Ishida, A., Nagase, T., and Rosing, M. T.: Evidence for biogenic graphite in early Archaean Isua metasedimentary rocks, Nature Geoscience, 7, 25–28, https://doi.org/10.1038/ngeo2025, 2014.

Otá lora, F., Mazurier, A., Garcia-Ruiz, J. M., Van Kranendonk, M., Kotopoulou, E., El Albani, A., and Garrido, C.: A crystallographic study of crystalline casts and pseudomorphs from the 3.5 Ga Dresser Formation, Pilbara Craton (Australia), Journal of Applied Crystallography, 51, 1050–1058, https://doi.org/10.1107/S1600576718007343, 2018.

845   Pratt, B. R.: Calcification of cyanobacterial filaments: *Girvanella* and the origin of lower Paleozoic lime mud, Geology, 29, 763—766, 2001.

Pei, Y.: A geobiological approach to carbonate factories and ecosystem changes across the Permian–Triassic boundary, Ph.D. thesis, University of Göttingen, Germany, http://dx.doi.org/10.53846/goediss-9160, 2022.

Pei, Y., Chen, Z.-Q., Fang, Y., Kershaw, S., Wu, S., and Luo, M.: Volcanism, redox conditions, and microbialite growth

850   linked with the end-Permian mass extinction: Evidence from the Xiajiacao section (western Hubei Province), South China, Palaeogeography, Palaeoclimatology, Palaeoecology, 519, 194–208, https://doi.org/10.1016/j.palaeo.2017.07.020, 2019.

Pei, Y., Duda, J.-P., and Reitner, J.: Sedimentary factories and ecosystem change across the Permian–Triassic Critical Interval (P–TrCI): insights from the Xiakou area (South China), PalZ, pp. 709–725, https://doi.org/10.1007/s12542-020-00530-x, 2021.

855   Pei, Y., Blumenberg, M., Duda, J.-P., Hö che, N., Peckmann, J., Birgel, D., Luo, J., Kment, K., and Reitner, J.: Ecosystem changes through the Permian–Triassic and Triassic–Jurassic critical intervals: Evidence from sedimentology, palaeontology and geochemistry, Sedimentology, https://doi.org/10.1111/sed.13088, 2023.

Perry, R. S. and Sephton, M. A.: Reply to comments on defining biominerals and organominerals: Direct and indirect indicators of life [Perry et al., Sedimentary Geology, 201, 157-179], Sedimentary Geology, 213, 156–156,

860   https://doi.org/10.1016/j.sedgeo.2008.11.005, 2009.

Perry, R. S., Mcloughlin, N., Lynne, B. Y., Sephton, M. A., Oliver, J. D., Perry, C. C., Campbell, K., Engel, M. H., Farmer, J. D., Brasier, M. D., and Staley, J.: Defining biominerals and organominerals: Direct and indirect indicators of life, Sedimentary Geology, 201, 157–179, https://doi.org/10.1016/j.sedgeo.2007.05.014, 2007.

Pinti, D. L., Hashizume, K., Sugihara, A., Massault, M., and Philippot, P.: Isotopic fractionation of nitrogen and carbon in

865   Paleoarchean cherts from Pilbara craton, Western Australia: Origin of 15N-depleted nitrogen, Geochimica et Cosmochimica Acta, 73, 3819–3848, https://doi.org/10.1016/j.gca.2009.03.014, 2009.

Pomar, L. and Hallock, P.: Carbonate factories: a conundrum in sedimentary geology, Earth-Science Reviews, 87, 134–169, https://doi.org/10.1016/j.earscirev.2007.12.002, 2008.

Pruss, S. B., Bottjer, D. J., Corsetti, F. A., and Baud, A.: A global marine sedimentary response to the end-Permian mass

870   extinction: examples from southern Turkey and the western United States, Earth-science reviews, 78, 193–206, https://doi.org/10.1016/j.earscirev.2006.05.002, 2006.

Rasmussen, B., Fletcher, I. R., and Muhling, J. R.: In situ U–Pb dating and element mapping of three generations of monazite: unravelling cryptic tectonothermal events in low-grade terranes, Geochimica et Cosmochimica Acta, 71, 670–690, https://doi.org/10.1016/j.gca.2006.10.020, 2007.

875   Reijmer, J. J.: Marine carbonate factories: review and update, Sedimentology, 68, 1729–1796, https://doi.org/10.1111/sed.12878, 2021.

Reitner, J.: Modern cryptic microbialite/metazoan facies from Lizard Island (Great Barrier Reef, Australia) formation and concepts, Facies, 29, 3-39, 1993.

Reitner, J.: Organomineralization: A clue to the understanding of meteorite-related "bacteria-shaped" carbonate particles, in:
880   Origins: Genesis, Evolution and Diversity of Life, pp. 195–212, Springer, 2004.

Reitner, J. and Neuweiler, F.: Part I Mud mounds: recognizing a polygenetic spectrum of fine-grained carbonate buildups, in:
Mudmounds: a polygenetic spectrum of fine-grained carbonate buildups, edited by Reitner, J. and Neuweiler, F., pp. 2–4,
1995.

Reitner, J. and Thiel, V.: Encyclopedia of Geobiology, Springer Amsterdam, 2011.

885   Reitner, J., Wilmsen, M., and Neuweiler, F.: Cenomanian/Turonian sponge microbialite deep-water hardground community
(Liencres, Northern Spain), Facies, 32, 203–212, https://doi.org/10.1007/BF02536869, 1995a.

Reitner, J., Neuweiler, F., and Gautret, P.: Part II Modern and fossil automicrites: implications for mud mound genesis, in:
Mud Mounds: A Polygenetic Spectrum of Fine-grained Carbonate Buildups, edited by Reitner, J. and Neuweiler, F., vol. 32,
pp. 4–17, 1995b.

890   Reitner, J., Gautret, P., Marin, F., and Neuweiler, F.: Automicrites in a modern marine microbialite. Formation model via
organic matrices (Lizard Island, Great Barrier Reef, Australia), Bulletin del'Institut océ anographique, Monaco, n° spé cial
14(2), 237–263, 1995c.

Reitner, J., Thiel, V., Zankl, H., Michaelis, W., Wö rheide, G., and Gautret, P.: Organic and biogeochemical patterns in
cryptic microbialites, in: Microbial sediments, edited by Riding, R. E. and Awramik, S. M., pp. 149–160, Springer, Berlin,
895   https://doi.org/10.1007/978-3-662-04036-2_17, 2000.

Reitner, J., Wö rheide, G., Lange, R., and Schumann-Kindel, G.: Coralline demosponges; a geobiological portrait,
Bulletin/The Tohoku University Museum, pp. 219–235, https://doi.org/10.23689/fidgeo-2565, 2001.

Riding, R.: The term stromatolite: towards an essential definition, Lethaia, 32, 321–330, https://doi.org/10.1111/j.1502-
3931.1999.tb00550.x, 1999.

900   Riding, R.: Microbial carbonates: the geological record of calcified bacterial–algal mats and biofilms, Sedimentology, 47,
179–214, https://doi.org/10.1046/j.1365-3091.2000.00003.x, 2000.

Rincó n-Tomá s, B., Khonsari, B., Mü hlen, D., Wickbold, C., Schä fer, N., Hause-Reitner, D., Hoppert, M., and Reitner,
J.: Manganese carbonates as possible biogenic relics in Archean settings, International Journal of Astrobiology, 15, 219–229,
https://doi.org/10.1017/S1473550416000264, 2016.

905   Robbins, L. and Blackwelder, P.: Biochemical and ultrastructural evidence for the origin of whitings: A biologically induced
calcium carbonate precipitation mechanism, Geology, 20, 464–468, https://doi.org/10.1130/0091-
7613(1992)020<0464:BAUEFT>2.3.CO;2, 1992.

Roberts, R. G.: Ore deposit models11. Archean lode gold deposits, Geoscience Canada, 14, 37–52,
https://id.erudit.org/iderudit/geocan14_1art02, 1987.

910   Rouillard, J., Van Kranendonk, M. J., Lalonde, S., Gong, J., and Van Zuilen, M. A.: Correlating trace element compositions,
petrol- ogy, and Raman spectroscopy data in the 3.46 Ga Apex chert, Pilbara Craton, Australia, Precambrian Research, 366,
106415, https://doi.org/10.1016/j.precamres.2021.106415, 2021.

Runge, E. A., Duda, J.-P., Van Kranendonk, M. J., and Reitner, J.: Earth's oldest tsunami deposit? Early Archaean high-energy sediments in the ca 3.48 Ga Dresser Formation (Pilbara, Western Australia), The Depositional Record, 8, 590–602,

915   https://doi.org/10.1002/dep2.175, 2022.

Schlager, W.: Sedimentation rates and growth potential of tropical, cool-water and mud-mound carbonate systems, Geological Society, London, Special Publications, 178, 217–227, https://doi.org/10.1144/GSL.SP.2000.178.01.14, 2000.

Schlager, W.: Benthic carbonate factories of the Phanerozoic, International Journal of Earth Sciences, 92, 445–464, https://doi.org/10.1007/s00531-003-0327-x, 2003.

920   Schopf, J. W.: Microfossils of the Early Archean Apex chert: new evidence of the antiquity of life, Science, 260, 640–646, https://doi.org/10.1126/science.260.5108.640, 1993.

Schopf, J. W., Kudryavtsev, A. B., Agresti, D. G., Wdowiak, T. J., and Czaja, A. D.: Laser–Raman imagery of Earth's earliest fossils, Nature, 416, 73–76, https://doi.org/10.1038/416073a, 2002.

Schopf, J. W., Kudryavtsev, A. B., Osterhout, J. T., Williford, K. H., Kitajima, K., Valley, J. W., and Sugitani, K.: An

925   anaerobic 3400 Ma shallow-water microbial consortium: Presumptive evidence of Earth's Paleoarchean anoxic atmosphere, Precambrian Research, 299, 309–318, https://doi.org/10.1016/j.precamres.2017.07.021, 2017.

Schrag, D. P., Higgins, J. A., Macdonald, F. A., and Johnston, D. T.: Authigenic carbonate and the history of the global carbon cycle, Science, 339, 540–543, https://doi.org/10.1126/science.1229578, 2013.

Sengupta, S., Peters, S. T., Reitner, J., Duda, J.-P., and Pack, A.: Triple oxygen isotopes of cherts through time, Chemical

930   Geology, 554, 119 789, https://doi.org/https://doi.org/10.1016/j.chemgeo.2020.119789, 2020.

Shibuya, T., Tahata, M., Kitajima, K., Ueno, Y., Komiya, T., Yamamoto, S., Igisu, M., Terabayashi, M., Sawaki, Y., Takai, K., et al.: Depth variation of carbon and oxygen isotopes of calcites in Archean altered upper oceanic crust: Implications for the CO_2 flux from ocean to oceanic crust in the Archean, Earth and Planetary Science Letters, 321, 64–73, https://doi.org/10.1016/j.epsl.2011.12.034, 2012.

935   Shields, G. A.: Implications of Carbonate and Chert Isotope Records for the Early Earth, in: Earth's Oldest Rocks, edited by Van Kranendonk, M., Bennett, V., and Hoffmann, J., pp. 901–912, Elsevier, 2019.

Smithies, R., Champion, D., and Cassidy, K.: Formation of Earth's early Archaean continental crust, Precambrian Research, 127, 89–101, https://doi.org/10.1016/S0301-9268(03)00182-7, 2003.

Smithies, R. H., Champion, D. C., Van Kranendonk, M. J., Howard, H. M., and Hickman, A. H.: Modern-style subduction

940   processes in the Mesoarchaean: geochemical evidence from the 3.12 Ga Whundo intra-oceanic arc, Earth and Planetary Science Letters, 231, 221–237, https://doi.org/10.1016/j.epsl.2004.12.026, 2005.

Smithies, R., Champion, D., Van Kranendonk, M., and Hickman, A.: Geochemistry of volcanic rocks of the northern Pilbara Craton, Western Australia, Geological Survey of Western Australia Report, 104, 1–47, 2007a.

Smithies, R. H., Champion, D. C., and Van Kranendonk, M. J.: The oldest well-preserved felsic volcanic rocks on Earth:

945   Geochemical clues to the early evolution of the Pilbara Supergroup and implications for the growth of a Paleoarchean

protocontinent, in: Earth's Oldest Rocks, edited by Van Kranendonk, M., Smithies, R., and Bennett, V., vol. Developments in Precambrian Geology 15, pp. 339–367, Elsevier, Amsterdam, https://doi.org/10.1016/S0166-2635(07)15042-8, 2007b.

Stockmann, G. J., Wolff-Boenisch, D., Gislason, S. R., and Oelkers, E. H.: Do carbonate precipitates affect dissolution kinetics? 1: Basaltic glass, Chemical Geology, 284, 306–316, https://doi.org/10.1016/j.chemgeo.2011.03.010, 2011.

950 Sugitani, K., Lepot, K., Nagaoka, T., Mimura, K., Van Kranendonk, M., Oehler, D. Z., and Walter, M. R.: Biogenicity of morphologically diverse carbonaceous microstructures from the ca. 3400 Ma Strelley Pool Formation, in the Pilbara Craton, Western Australia, Astrobiology, 10, 899–920, https://doi.org/10.1089/ast.2010.0513, 2010.

Sugitani, K., Mimura, K., Nagaoka, T., Lepot, K., and Takeuchi, M.: Microfossil assemblage from the 3400 Ma Strelley Pool Formation in the Pilbara Craton, Western Australia: results form a new locality, Precambrian Research, 226, 59–74,
955 https://doi.org/10.1016/j.precamres.2012.11.005, 2013.

Sugitani, K., Mimura, K., Takeuchi, M., Yamaguchi, T., Suzuki, K., Senda, R., Asahara, Y., Wallis, S., and Van Kranendonk, M.: A Paleoarchean coastal hydrothermal field inhabited by diverse microbial communities: the Strelley Pool Formation, Pilbara Craton, Western Australia, Geobiology, 13, 522–545, https://doi.org/10.1111/gbi.12150, 2015a.

Sugitani, K., Mimura, K., Takeuchi, M., Lepot, K., Ito, S., and Javaux, E.: Early evolution of large micro-organisms with
960 cytological complexity revealed by microanalyses of 3.4 Ga organic-walled microfossils, Geobiology, 13, 507–521, https://doi.org/10.1111/gbi.12148, 2015b.

Sugitani, K., Kohama, T., Mimura, K., Takeuchi, M., Senda, R., and Morimoto, H.: Speciation of Paleoarchean life demonstrated by analysis of the morphological variation of lenticular microfossils from the Pilbara Craton, Australia, Astrobiology, 18, 1057–1070, https://doi.org/10.1089/ast.2017.1799, 2018.

965 Taylor, S. R. and McLennan, S.: The composition and evolution of the continental crust: rare earth element evidence from sedimentary rocks, Philosophical Transactions of the Royal Society of London. Series A, Mathematical and Physical Sciences, 301, 381–399, https://doi.org/10.1098/rsta.1981.0119, 1981.

Terabayashi, M., Masada, Y., and Ozawa, H.: Archean ocean-floor metamorphism in the North Pole area, Pilbara Craton, western Australia, Precambrian Research, 127, 167–180, https://doi.org/10.1016/S0301-9268(03)00186-4, 2003.

970 Thompson, J. B., Schultze-Lam, S., Beveridge, T. J., and Des Marais, D. J.: Whiting events: biogenic origin due to the photosynthetic activity of cyanobacterial picoplankton, Limnology and oceanography, 42, 133–141, https://doi.org/10.4319/lo.1997.42.1.0133, 1997.

Thorpe, R., Hickman, A., Davis, D., Mortensen, J., and Trendall, A.: U-Pb zircon geochronology of Archaean felsic units in the Marble Bar region, Pilbara Craton, Western Australia, Precambrian Research, 56, 169–189, https://doi.org/10.1016/0301-
975 9268(92)90100-3, 1992.

Tice, M. M., Thornton, D. C., Pope, M. C., Olszewski, T. D., and Gong, J.: Archean microbial mat communities, Annual review of earth and planetary sciences, 39, 297–319, https://doi.org/10.1146/annurev-earth-040809-152356, 2011.

Trichet, J. and Défarge, C.: Non-biologically supported organomineralization, Bulletin de l'Institut océanographique, Monaco. Numéro special 14(2), 203–236, 1995.

980   Ueno, Y., Isozaki, Y., Yurimoto, H., and Maruyama, S.: Carbon isotopic signatures of individual Archean microfossils (?) from Western Australia, International Geology Review, 43, 196–212, https://doi.org/10.1080/00206810109465008, 2001.

Ueno, Y., Yoshioka, H., Maruyama, S., and Isozaki, Y.: Carbon isotopes and petrography of kerogens in 3.5-Ga hydrothermal silica dikes in the North Pole area, Western Australia, Geochimica et Cosmochimica Acta, 68, 573–589, https://doi.org/10.1016/S0016-7037(03)00462- 9, 2004.

985   van den Boorn, S. H., van Bergen, M. J., Nijman, W., and Vroon, P. Z.: Dual role of seawater and hydrothermal fluids in Early Archean chert formation: evidence from silicon isotopes, Geology, 35, 939–942, https://doi.org/10.1130/G24096A.1, 2007.

Van Kranendonk, M. J.: Volcanic degassing, hydrothermal circulation and the flourishing of early life on Earth: A review of the evidence from c. 3490-3240 Ma rocks of the Pilbara Supergroup, Pilbara Craton, Western Australia, Earth-Science
990   Reviews, 74, 197–240, https://doi.org/10.1016/j.earscirev.2005.09.005, 2006.

Van Kranendonk, M. J.: A review of the evidence for putative Paleoarchean life in the Pilbara Craton, Western Australia, Developments in Precambrian Geology, 15, 855–877, https://doi.org/10.1016/S0166-2635(07)15072-6, 2007.

Van Kranendonk, M.: Stromatolite morphology as an indicator of biogenicity for Earth's oldest fossils from the 3.5-3.4 Ga Pilbara Craton, Western Australia, in: Advances in stromatolite geobiology. Lecture notes in earth sciences, edited by
995   Reitner, J., Queric, N., and Arp, G., vol. 131, pp. 517–534, 2011.

Van Kranendonk, M. J. and Pirajno, F.: Geochemistry of metabasalts and hydrothermal alteration zones associated with c. 3.45 Ga chert and barite deposits: implications for the geological setting of the Warrawoona Group, Pilbara Craton, Australia, Geochemistry: Exploration, Environment, Analysis, 4, 253–278, https://doi.org/10.1144/1467-7873/04-205, 2004.

Van Kranendonk, M. J., Hickman, A. H., Smithies, R. H., Nelson, D. R., and Pike, G.: Geology and tectonic evolution of the
1000   Archean North Pilbara terrain, Pilbara Craton, Western Australia, Economic Geology, 97, 695–732, https://doi.org/10.2113/gsecongeo.97.4.695, 2002.

Van Kranendonk, M. J., Webb, G. E., and Kamber, B. S.: Geological and trace element evidence for a marine sedimentary environment of deposition and biogenicity of 3.45 Ga stromatolitic carbonates in the Pilbara Craton, and support for a reducing Archaean ocean, Geobiology, 1, 91–108, https://doi.org/10.1046/j.1472-4669.2003.00014.x, 2003.

1005   Van Kranendonk, M. J., Hickman, A. H., and Huston, D. L.: Geology and Mineralization of the East Pilbara d A Field Guide, Western Australia Geological Survey. Record 2006/16, 94p, 2006.

Van Kranendonk, M. J., Hugh Smithies, R., Hickman, A. H., and Champion, D.: Secular tectonic evolution of Archean continental crust: interplay between horizontal and vertical processes in the formation of the Pilbara Craton, Australia, Terra Nova, 19, 1–38, https://doi.org/10.1111/j.1365-3121.2006.00723.x, 2007a.

1010   Van Kranendonk, M. J., Smithies, R. H., Hickman, A. H., and Champion, D. C.: Paleoarchean development of a continental nucleus: the East Pilbara terrane of the Pilbara craton, Western Australia, Developments in Precambrian geology, 15, 307–337, https://doi.org/10.1016/S0166-2635(07)15041-6, 2007b.

Van Kranendonk, M. J., Philippot, P., Lepot, K., Bodorkos, S., and Pirajno, F.: Geological setting of Earth's oldest fossils in the ca. 3.5 Ga Dresser formation, Pilbara Craton, Western Australia, Precambrian Research, 167, 93–124, https://doi.org/10.1016/j.precamres.2008.07.003, 2008.

Van Kranendonk, M. J., Smithies, R. H., Hickman, A. H., and Champion, D. C.: Paleoarchean development of a continental nucleus: the East Pilbara Terrane of the Pilbara Craton, Western Australia, in: Earth's Oldest Rocks, edited by Van Kranendonk, M.J., Bennett, V.C., Hoffmann, J.E., pp. 437–462, Elsevier, 2019a.

Van Kranendonk, M., Djokic, T., Poole, G., Tadbiri, S., Steller, L., and Baumgartner, R.: Depositional Setting of the Fossiliferous, c.3480 Ma Dresser Formation, Pilbara Craton: A Review, in: Earth's Oldest Rocks, edited by Van Kranendonk, M.J., Bennett, V.C., Hoffmann, J.E., pp. 985–1006, Elsevier, 2019b.

van Zuilen, M. A.: Proposed early signs of life not set in stone, Nature, pp. 190–191, https://doi.org/10.1038/d41586-018-06994-x, 2018.

van Zuilen, M.: The Significance of Carbonaceous Matter to Understanding Life Processes on Early Earth. In: Van Kranendonk, M.J., Bennett, V.C., Hoffmann, J.E. (Eds.), in: Earth's Oldest Rocks. Elsevier, 945–963, 2019.

Veizer, J., Hoefs, J., Ridler, R., Jensen, L., and Lowe, D.: Geochemistry of Precambrian carbonates: I. Archean hydrothermal systems, Geochimica et Cosmochimica Acta, 53, 845–857, https://doi.org/10.1016/0016-7037(89)90030-6, 1989a.

Veizer, J., Hoefs, J., Lowe, D., and Thurston, P.: Geochemistry of Precambrian carbonates: II. Archean greenstone belts and Archean sea water, Geochimica et Cosmochimica Acta, 53, 859–871, https://doi.org/10.1016/0016-7037(89)90031-8, 1989b.

Viehmann, S., Reitner, J., Tepe, N., Hohl, S. V., Van Kranendonk, M., Hofmann, T., Koeberl, C., and Meister, P.: Carbonates and cherts as archives of seawater chemistry and habitability on a carbonate platform 3.35 Ga ago: Insights from Sm/Nd dating and trace element analysis from the Strelley Pool Formation, Western Australia, Precambrian Research, 344, 105742, https://doi.org/10.1016/j.precamres.2020.105742, 2020.

Voigt, M., Pearce, C. R., Baldermann, A., and Oelkers, E. H.: Stable and radiogenic strontium isotope fractionation during hydrothermal seawater-basalt interaction, Geochimica et Cosmochimica Acta, 240, 131–151, https://doi.org/10.1016/j.gca.2018.08.018, 2018.

Wacey, D.: Stromatolites in the 3400 Ma Strelley Pool Formation, Western Australia: examining biogenicity from the macro-to the nano- scale, Astrobiology, 10, 381–395, https://doi.org/10.1089/ast.2009.0423, 2010.

Wacey, D., McLoughlin, N., Whitehouse, M. J., and Kilburn, M. R.: Two coexisting sulfur metabolisms in a ca. 3400 Ma sandstone, Geology, 38, 1115–1118, https://doi.org/10.1130/G31329.1, 2010.

Wacey, D., Kilburn, M. R., Saunders, M., Cliff, J., and Brasier, M. D.: Microfossils of sulphur-metabolizing cells in 3.4-billion-year-old rocks of Western Australia, Nature Geoscience, 4, 698–702, https://doi.org/10.1038/ngeo1238, 2011.

Wacey, D., Noffke, N., Saunders, M., Guagliardo, P., and Pyle, D. M.: Volcanogenic pseudo-fossils from the 3.48 Ga dresser formation, Pilbara, Western Australia, Astrobiology, 18, 539–555, https://doi.org/10.1089/ast.2017.1734, 2018.

Wang, J., Tarhan, L. G., Jacobson, A. D., Oehlert, A. M., and Planavsky, N. J.: The evolution of the marine carbonate factory, Nature, pp. 1–5, https://doi.org/10.1038/s41586-022-05654-5, 2023.

Weiner, S. and Dove, P. M.: An overview of biomineralization processes and the problem of the vital effect, Reviews in mineralogy and geochemistry, 54, 1–29, https://doi.org/10.2113/0540001, 2003.

Wojdyr, M.: Fityk: a general-purpose peak fitting program, Journal of Applied Crystallography, 43, 1126–1128,
1050 https://doi.org/10.1107/S0021889810030499, 2010.

Wolff-Boenisch, D. and Galeczka, I.: Flow-through reactor experiments on basalt-(sea)water-CO_2 reactions at 90 °C and neutral pH. What happens to the basalt pore space under post-injection conditions?, International Journal of Greenhouse Gas Control, 68, 176–190, https://doi.org/10.1016/j.ijggc.2017.11.013, 2018.

Xiang, W.: Carbonate factories in the early Archean and their geobiological impacts, Ph.D. thesis, University of Göttingen,
1055 Germany, http://dx.doi.org/10.53846/goediss-10047, 2023.

Xiong, W., Wells, R. K., Horner, J. A., Schaef, H. T., Skemer, P. A., and Giammar, D. E.: CO_2 mineral sequestration in naturally porous basalt, Environmental Science & Technology Letters, 5, 142–147, https://doi.org/10.1021/acs.estlett.8b00047, 2018.

Yamamoto, K., Itoh, N., Matsumoto, T., Tanaka, T., and Adachi, M.: Geochemistry of Precambrian carbonate intercalated in
1060 pillows and its host basalt: implications for the REE composition of circa 3.4 Ga seawater, Precambrian Research, 135, 331–344, https://doi.org/10.1016/j.precamres.2004.09.006, 2004.

Zawaski, M. J., Kelly, N. M., Orlandini, O. F., Nichols, C. I., Allwood, A. C., and Mojzsis, S. J.: Reappraisal of purported ca. 3.7 Ga stromatolites from the Isua Supracrustal Belt (West Greenland) from detailed chemical and structural analysis, Earth and Planetary Science Letters, 545, 116 409, https://doi.org/10.1016/j.epsl.2020.116409, 2020.

1065 Zawaski, M. J., Kelly, N. M., Orlandini, O. F., Nichols, C. I., Allwood, A. C., and Mojzsis, S. J.: Reply: The Isua (Greenland)" relict stromatolites" cannot be confidently interpreted as original sedimentary structures, Earth and Planetary Science Letters, 562, 116 851, https://doi.org/10.1016/j.epsl.2021.116851, 2021.

1070